Title
The Structural Basis of Yeast Prion Strain Variants

Author
Toyama, Brandon Hiroyuki

Publication Date
2009

Peer reviewed|Thesis/dissertation

The Structural Basis of Yeast Prion Strain Variants

by

Brandon Hiroyuki Toyama

DISSERTATION

Submitted in partial satisfaction of the requirements for the degree of

DOCTOR OF PHILOSOPHY

in

Biochemistry

in the

GRADUATE DIVISION

of the

UNIVERSITY OF CALIFORNIA, SAN FRANCISCO

For my family and Erin

Acknowledgments

While interviewing for graduate school in the late winter of 2003, I could sense that there was something unique about UCSF that no other graduate school could offer. After being accepted into the Tetrad program, I knew immediately that if I declined, I would regret it. I could see myself constantly asking "what if…?" anytime something went wrong if I was not at UCSF. This sense of impending regret is something I didn't feel about any other graduate school I interviewed at, and accordingly, have not regretted my decision for any moment here, good or bad. This happiness and satisfaction, of course, is not the product of myself, rather, it is a product of all the wonderful people that I have had the pleasure to associate with at UCSF.

Thanks firstly to Peter Walter, who was my host during my UCSF interview. Peter is largely responsible for why I came to UCSF. His excitement about science and his relaxed and fun relationship with students is very representative of the "something unique" at UCSF that made it clear that this was the place for me. His help with my post-doc search and interest in where I will end up also illustrates his care and pride in the students at UCSF.

Thanks to all the people that deal with the technical, administrative, and support stuff that I would have forgotten had they not been there. This includes Sue Adams, Danny Dam, Rachel Mozesson and others, past and present, in the Tetrad office. Alice Willis in the lab, who has processed countless receipts for me and provided many unnecessary, but

appreciated, sources of bad calories. Manny and Lily who make the lab mysteriously run, a fact we only remember when they go on vacation.

Thanks to the many UCSF faculty that have helped me along the way. Jeff Cox and Geeta Narlikar, my Tetrad journal club coaches, for learning how to better present science in front of an audience. Hiten Madhani, David Agard, Carol Gross, and Tanja Kortemme, my orals committee, for teaching me how to better think about science, be more critical, think better on my feet, and the importance of knowing your project better than anyone else in the world (or at least the room)…and for passing me. David Agard, John Gross, and Mark Kelly, my thesis committee, for helping guide me through my project and graduate career, providing helpful suggestions, and showing a genuine interest in me and my work.

I would also like to again thank Mark Kelly, a collaborator for much of my time at UCSF. Mark has taught me everything I know about NMR with incredible patience and disregard for his own time. He has always found time to help and explain the inner workings of NMR to me, including the frantic time leading up to my qualifying exam. I wasn't excited about NMR before coming here, but now, because of Mark, I look forward to using NMR in my future studies. Mark has also provided endless entertaining and helpful stories of "the bad old days of NMR", skiing conditions around the world, places to see in Berlin, and many many other topics.

A big thanks goes out to my classmates. I couldn't ask for a better, more fun and entertaining class that like to bring way too much food to events. In particular, I would like to thank Tetsuya Matsuguchi (pudd'n tets) for playing monopoly, eating sushi and trying to make a failed review website with me, playing rockband, participating in various food adventures, and many other things that have prevented me from graduating earlier. You've been a great friend, and educator of Japanese culture that I have missed. Victoria Newman, for providing endless entertaining stories, about herself or others, that make me gasp, laugh, and puke a little in my mouth. Monica Rodrigo-Brenni, for having tea with us, taking us around Chile, and making grad-school more fun. Brad Green and Kevin Jones, for playing basketball and fantasy sports and getting Brad so angry in basketball that he threw his shoe down the court. Claire Rowe, for asking the questions we all want to ask, but were too afraid or timid to do. Stacy Chen, for adventures in vegan cooking and taking me and Tet to Japantown, even when she didn't need anything. Janet Yang, for providing great ideas and fun into many creative projects.

Thanks also to the lab, past and present, for providing a fun and helpful environment to grow as a scientist. I would like to thank all members of the [*PSI*$^{+}$] group that helped me, Peter Chien, Angela DePace, Motomasa Tanaka (Moto), Kim Tipton, Sean Collins, Clement Chu, Dale Cameron, Katie Verges, and Cat Foo, and my great bay mates over the years, Moto, Kim, Katie, Edwin Rodriguez (my new lab little brother that I get to pick on with great pleasure), and Nick Ingolia.

In particular, I would like to thank the following labmates:

Moto taught me so much as a starting graduate student, was a wonderful benchmate, and the consummate scientist to look up to. He was quiet most of the time, which was great, but also quick to talk about science, Japanese things, or baseball. He was greatly missed when he left to start his own lab.

Clement was someone I could easily talk to since we have so many things in common (so I think), including massive biceps. He was a great person to talk science with, but also golf, sports, technology, computers, coffee, beer, food, and just about any subject you can think of, he knows something about it. How many other people do you know that not only have heard of a "grande meal", but know where to get it and have eaten it all (it is meant to serve a small family) in one sitting multiple times? He has generously provided countless rides to food and activities. He has also provided a large amount of guilt when going home from lab. There was one night when I was packing up to go home around 12:30am. He saw me, and gave me that look of "where do you think you are going this early?" Ignoring this, I proceeded downstairs to get a taxi voucher to go home, where I was met with a "why are you going home so early?" from the security guard. When the taxi finally arrived, I got in, only to again be met with a "what are you doing? You aren't allowed to go home this early!" from the cab driver. He was one of my "usual" drivers. Clement must have had something to do with this I'm convinced.

David Breslow, I admit, is pretty funny, especially when it comes at the expense of lab mates that aren't me. Despite what he thinks, he is the male version of Erin. Conversations I have had with Dave were identical to ones I've had with Erin a year

earlier, substituting “Orm” with “Yos9”. He’s really been enjoyable to be in lab with, extremely sharp in both his intellect and his wit.

Cat Foo has increased my enjoyment of lab substantially. A really fun person to hang out with, armed with countless funny but true stories, always up for participating in some sort of adventure. I’ve been really happy that we got to work together so much.

Sean Collins was my fantasy sports buddy in lab, among other things. I have missed being able to talk to someone about a trade I am trying to make or what a great game my third baseman had. No one else in the lab has nearly a strong appreciation for the great thing that is fantasy sports as Sean.

Katie Verges has been a great classmate and buddy in the [*PSI*] group. She was always willing to help when help was needed, and was someone you could really count on. It is always great to have other people at the same stage, trying to navigate graduate school with you.

Kim Tipton was a very positive influence when deciding if I wanted to join the Weissman lab. She was also a great “older sister” figure in the lab, showing us how to think about prion biology, how to do the various prion assays, and how to interact with Jonathan, all with incredible patience. She was a great example to learn from.

Vlad Denic never ceased to make me laugh. No one could roll with the punches quite like him. On top of that, he is a great scientist, and another person to look up to and learn from, even if it is what not to do when dating someone within the lab.

I would also like to thank my family, Ron and Joanne Toyama, Nikki Toyama-Szeto, Jesse and Alaina Szeto, Katherine and Jason Solverson, including my new family, Erin Quan Toyama, Harvey and Suey Quan, and Tracy Quan, who have all been instrumental in my education and journey through grad school. My parents (Ron and Joanne), have always been supportive of any academic endeavor I pursued, whether it involved buying out an entire store's worth of plaster of paris, driving around in search for an obscene number of magnets, or going to the home of a Northwestern professor late at night to discuss doing "sleep" research in his lab. They have provided the complete freedom to pursue any academic path I chose, and met it with support and pride. I couldn't ask for anything more. My sisters have also been similarly supportive and encouraging, however, also poised to quickly make fun of me or give me a hard time at any opportune time. Their husbands have been a welcomed addition to the family, and provide a much needed male balance to the family dinner table. Although Alaina now tips that balance back, I'll excuse it because she is too cute. My new parents-in-law, Harvey and Suey, have always showed me the utmost hospitality despite the fact that I threatened to take their daughter away. More than that, they are well aware of my love for food, and consequently, enable and provide many culinary adventures when we visit. Tracy has also been great to get-to-know, providing a nice additional scientific perspective into conversations. Finally, there is Erin. Of all the things to do in graduate school, finding a

wife was one that I wasn't expecting. In the same lab nonetheless. This was in fact, ill advised, and I wish I saw the look of shock/horror on Jonathan's face when he learned we were dating. But we did it. And in fine fashion if I might say so myself. A great scientist, person, friend, and now wife, I couldn't imagine going through grad school or the Weissman lab without her. And now I get to take the best part of the Weissman lab with me when I move on.

I finally would like to of course acknowledge Jonathan Weissman. Many people have written many words describing the numerous positive qualities and peculiarities of Jonathan, so I will try to be brief. Jonathan is an incredibly bright and creative scientist, possessing the gift of being able to convince you how interesting and important a particular story is, and has this uncanny ability to see what the next up and coming topic or technique will be. More than these things, however, I have really appreciated his consideration and respect for everyone in the lab, from a starting first year graduate student to an experienced postdoc. I remember, particularly in my early days in the lab, meeting with Jonathan and him asking me, "what do you think?" regarding some scientific issue. Not only would he then proceed to listen to my poorly conceived and crafted opinion, but would often take what I said, acknowledge it, mold it into a much better point than I intended, state it in a far more eloquent manner, and then give me credit for it. The same consideration was evident when helping him review papers, as he not only wanted my opinion on the paper, but also advice on how to precisely word a response. Someone so smart and experienced could have rightfully done what he wanted without any external input, but the genuine value and respect he places on the people of

his lab make him not only a talented scientist, but a great person as well. Unbeknownst to me when I decided to join the lab, I have had the pleasure of working for a great model scientist to attempt to emulate as I pursue my own scientific career.

Abstract

This study aimed to establish a better understanding of the structural basis of yeast prion strains. Prions are infectious agents that are comprised solely of protein, completely devoid of nucleic acid. This protein-only model, however, initially had its share of skeptics who pointed to disease phenomenon that could not be explained by a proteinaceous infectious agent. The existence of different strains was one such phenomenon that provided a formidable challenge to the protein-only prion hypothesis. How could a protein-only infectious agent cause different disease phenotypes in genetically identical animals? The explanation for this strain phenomenon was that there existed multiple infectious conformations of the prion protein, each of which corresponded to a specific disease manifestation. Although there was increasing evidence for multiple infectious conformations of the prion protein, the comprehensive connection from prion conformation to *in vivo* phenotype would most likely come from the more simple model yeast prion [*PSI*]. In these studies, I describe this yeast system and our structural studies that probed the conformational and physical differences between the aggregates responsible for two different strain phenotypes. Initial studies established that these two different prion strains, called Sc4 and Sc37, were indeed caused by two different conformations of aggregate. Our studies then established that these two conformations were physically distinct, the Sc4 conformation polymerizing slower but resulting in a physically weaker fiber and the Sc37 conformation polymerizing quickly into a strong and ridged structure. Our subsequent studies used hydrogen/deuterium exchange NMR and mutagenesis two map out in detail the conformational differences between Sc4 and Sc37 fibers. This study found that the Sc4

conformation represented a small core structure, while the Sc37 conformation represented an almost doubling of core structure. These data provided a structural rationale for the observed physical differences between Sc4 and Sc37 aggregates. Thus, a full explanation of how conformational heterogeneity can lead to distinct *in vivo* phenotypes is now possible.

Contributions

Portions of the text and figures presented in this thesis are reproduced with permission from material published previously. Chapter 2 "The physical basis of how prion conformations determine strain phenotypes" was published August 3rd 2006 in Nature Vol. 442, pp. 585-9. Dr. Motomasa Tanaka initiated this work, performed all bulk fiber polymerization assays, fiber fragmentation assays, sedimentation assays, *in vivo* infection and propagon counting assays, and aggregate size assays. Dr. Sean R. Collins developed the mathematical models for this work. Chapter 3 "The structural basis of yeast prion strain variants" was published September 13th 2007 in Nature Vol. 449 pp. 233-7. Dr. Mark J.S. Kelly assisted in setting up NMR experiments and NMR data analysis. Dr. John D. Gross assisted in the planning and execution of performing NMR on fibers in solution as well as some experiments that were not published. Dr. Mark J.S. Kelly also assisted with setting up NMR experiments and data analysis in "Oligomers of SupNM" in chapter 4. With the exception of those items listed above, the work presented in this thesis was performed by its author, Brandon H. Toyama, under the supervision of Dr. Jonathan S. Weissman.

Permissions

NATURE PUBLISHING GROUP LICENSE TERMS AND CONDITIONS

Aug 29, 2009

This is a License Agreement between Brandon H Toyama ("You") and Nature Publishing Group ("Nature Publishing Group") provided by Copyright Clearance Center ("CCC"). The license consists of your order details, the terms and conditions provided by Nature Publishing Group, and the payment terms and conditions.

All payments must be made in full to CCC. For payment instructions, please see information listed at the bottom of this form.

License Number	2258411111343
License date	Aug 29, 2009
Licensed content publisher	Nature Publishing Group
Licensed content publication	Nature
Licensed content title	The physical basis of how prion conformations determine strain phenotypes
Licensed content author	Motomasa Tanaka, Sean R. Collins, Brandon H. Toyama, Jonathan S. Weissman
Volume number	
Issue number	
Pages	
Year of publication	2006
Portion used	Full paper
Requestor type	Student
Type of Use	Thesis / Dissertation
Billing Type	Invoice
Company	Brandon H Toyama
Billing Address	1700 4th St. Byers Hall room 404 San Francisco, CA 94158 United States
Customer reference info	
Total	0.00 USD
Terms and Conditions	

Terms and Conditions for Permissions

Nature Publishing Group hereby grants you a non-exclusive license to reproduce this material for this purpose, and for no other use, subject to the conditions below:

1. NPG warrants that it has, to the best of its knowledge, the rights to license reuse of this material. However, you should ensure that the material you are requesting is original to Nature Publishing Group and does not carry the copyright of another entity (as credited in the published version). If the credit line on any part of the material you have requested indicates that it was reprinted or adapted by NPG with permission from another source, then you should also seek permission from that source to reuse the material.

2. Permission granted free of charge for material in print is also usually granted for any electronic version of that work, provided that the material is incidental to the work as a whole and that the electronic version is essentially equivalent to, or substitutes for, the print version. Where print permission has been granted for a fee, separate permission must be obtained for any additional, electronic re-use (unless, as in the case of a full paper, this has already been accounted for during your initial request in the calculation of a print run). NB: In all cases, web-based use of full-text articles must be authorized separately through the 'Use on a Web Site' option when requesting permission.

3. Permission granted for a first edition does not apply to second and subsequent editions and for editions in other languages (except for signatories to the STM Permissions Guidelines, or where the first edition permission was granted for free).

4. Nature Publishing Group's permission must be acknowledged next to the figure, table or abstract in print. In electronic form, this acknowledgement must be visible at the same time as the figure/table/abstract, and must be hyperlinked to the journal's homepage.
5. The credit line should read:

   Reprinted by permission from Macmillan Publishers Ltd: [JOURNAL NAME] (reference citation), copyright (year of publication)

   For AOP papers, the credit line should read:

   Reprinted by permission from Macmillan Publishers Ltd: [JOURNAL NAME], advance online publication, day month year (doi: 10.1038/sj.[JOURNAL ACRONYM].XXXXX)

6. Adaptations of single figures do not require NPG approval. However, the adaptation should be credited as follows:

   Adapted by permission from Macmillan Publishers Ltd: [JOURNAL NAME] (reference citation), copyright (year of publication)

7. Translations of 401 words up to a whole article require NPG approval. Please visit

http://www.macmillanmedicalcommunications.com for more information. Translations of up to a 400 words do not require NPG approval. The translation should be credited as follows:

Translated by permission from Macmillan Publishers Ltd: [JOURNAL NAME] (reference citation), copyright (year of publication).

We are certain that all parties will benefit from this agreement and wish you the best in the use of this material. Thank you.

v1.1

Gratis licenses (referencing $0 in the Total field) are free. Please retain this printable license for your reference. No payment is required.

If you would like to pay for this license now, please remit this license along with your payment made payable to "COPYRIGHT CLEARANCE CENTER" otherwise you will be invoiced within 30 days of the license date. Payment should be in the form of a check or money order referencing your account number and this license number 2258411111343.
If you would prefer to pay for this license by credit card, please go to http://www.copyright.com/creditcard to download our credit card payment authorization form.

Make Payment To:
Copyright Clearance Center
Dept 001
P.O. Box 843006
Boston, MA 02284-3006

If you find copyrighted material related to this license will not be used and wish to cancel, please contact us referencing this license number 2258411111343 and noting the reason for cancellation.

Questions? customercare@copyright.com or +1-877-622-5543 (toll free in the US) or +1-978-646-2777.

NATURE PUBLISHING GROUP LICENSE TERMS AND CONDITIONS

Aug 29, 2009

This is a License Agreement between Brandon H Toyama ("You") and Nature Publishing Group ("Nature Publishing Group") provided by Copyright Clearance Center ("CCC"). The license consists of your order details, the terms and conditions provided by Nature Publishing Group, and the payment terms and conditions.

All payments must be made in full to CCC. For payment instructions, please see information listed at the bottom of this form.

License Number	2258411004015
License date	Aug 29, 2009
Licensed content publisher	Nature Publishing Group
Licensed content publication	Nature
Licensed content title	The structural basis of yeast prion strain variants
Licensed content author	Brandon H. Toyama , Mark J. S. Kelly , John D. Gross and Jonathan S. Weissman
Volume number	449
Issue number	7159
Pages	pp233-237
Year of publication	2007
Portion used	Full paper
Requestor type	Student
Type of Use	Thesis / Dissertation
Billing Type	Invoice
Company	Brandon H Toyama
Billing Address	1700 4th St. Byers Hall room 404 San Francisco, CA 94158 United States
Customer reference info	
Total	0.00 USD
Terms and Conditions	

Terms and Conditions for Permissions

Nature Publishing Group hereby grants you a non-exclusive license to reproduce this material for this purpose, and for no other use, subject to the conditions below:

1. NPG warrants that it has, to the best of its knowledge, the rights to license reuse of this material. However, you should ensure that the material you are requesting is original to Nature Publishing Group and does not carry the copyright of another entity (as credited in the published version). If the credit line on any part of the material you have requested indicates that it was reprinted or adapted by NPG with permission from another source, then you should also seek permission from that source to reuse the material.

2. Permission granted free of charge for material in print is also usually granted for any electronic version of that work, provided that the material is incidental to the work as a whole and that the electronic version is essentially equivalent to, or substitutes for, the print version. Where print permission has been granted for a fee, separate permission must be obtained for any additional, electronic re-use (unless, as in the case of a full paper, this has already been accounted for during your initial request in the calculation of a print run). NB: In all cases, web-based use of full-text articles must be authorized separately through the 'Use on a Web Site' option when requesting permission.

3. Permission granted for a first edition does not apply to second and subsequent editions and for editions in other languages (except for signatories to the STM Permissions Guidelines, or where the first edition permission was granted for free).

4. Nature Publishing Group's permission must be acknowledged next to the figure, table or abstract in print. In electronic form, this acknowledgement must be visible at the same time as the figure/table/abstract, and must be hyperlinked to the journal's homepage.
5. The credit line should read:

   Reprinted by permission from Macmillan Publishers Ltd: [JOURNAL NAME] (reference citation), copyright (year of publication)

   For AOP papers, the credit line should read:

   Reprinted by permission from Macmillan Publishers Ltd: [JOURNAL NAME], advance online publication, day month year (doi: 10.1038/sj.[JOURNAL ACRONYM].XXXXX)

6. Adaptations of single figures do not require NPG approval. However, the adaptation should be credited as follows:

   Adapted by permission from Macmillan Publishers Ltd: [JOURNAL NAME] (reference citation), copyright (year of publication)

7. Translations of 401 words up to a whole article require NPG approval. Please visit

http://www.macmillanmedicalcommunications.com for more information. Translations of up to a 400 words do not require NPG approval. The translation should be credited as follows:

Translated by permission from Macmillan Publishers Ltd: [JOURNAL NAME] (reference citation), copyright (year of publication).

We are certain that all parties will benefit from this agreement and wish you the best in the use of this material. Thank you.

v1.1

Gratis licenses (referencing $0 in the Total field) are free. Please retain this printable license for your reference. No payment is required.

If you would like to pay for this license now, please remit this license along with your payment made payable to "COPYRIGHT CLEARANCE CENTER" otherwise you will be invoiced within 30 days of the license date. Payment should be in the form of a check or money order referencing your account number and this license number 2258411004015.
If you would prefer to pay for this license by credit card, please go to http://www.copyright.com/creditcard to download our credit card payment authorization form.

Make Payment To:
Copyright Clearance Center
Dept 001
P.O. Box 843006
Boston, MA 02284-3006

If you find copyrighted material related to this license will not be used and wish to cancel, please contact us referencing this license number 2258411004015 and noting the reason for cancellation.

Questions? customercare@copyright.com or +1-877-622-5543 (toll free in the US) or +1-978-646-2777.

Table of Contents

List of Figures

Chapter 2

Chapter 3

Chapter 4

Chapter 1

Introduction

Introduction

A Prion, as described by Stanley Prusiner in 1982, is "a small proteinaceous infectious particle which is resistant to inactivation by most procedures that modify nucleic acids"(Prusiner, 1982). Initially allowing the presence of a small amount of nucleic acid, the prion hypothesis evolved to more narrowly describe the infectious agent as composed solely of protein (the prion protein Prp) and is completely devoid of nucleic acid (Cohen and Prusiner, 1998). As a genome-less pathogen was a lengthy divergence from known infectious agents at the time such as bacteria and viruses, the prion protein-only hypothesis has had a tumultuous journey to widespread acceptance.

Perhaps one of the more compelling arguments against the prion hypothesis was the existence of strains in prion diseases. Strains were first observed as different isolates of the infectious agent that gave rise to different disease phenotypes in the form of incubation times and histopathology when introduced into genetically identical animals (Dickinson and Meikle, 1969). Different disease strains are easily explained by differences in the infectious agent's genome. However, in the absence of any nucleic acid genome, as was proposed to be the case with prions, how could different strains possibly arise? This was a large part of an argument against the protein-only hypothesis when in 1987 Bruce and Dickinson wrote in regards to the scrapie prion in sheep, "The considerable strain diversity in scrapie, together with the evidence for mutational change presented here and elsewhere, offer compelling arguments that scrapie has its own independently replicating genome" (Bruce and Dickinson, 1987). Experiments with two different strains of prion-based transmissible mink encephalopathy (TME), however,

offered a possible explanation for this phenomenon. Bessen and Marsh found that the infectious agent that caused the Drowsy (Dy) and Hyper (HY) strains in TME had different sensitivities to proteases despite being made up of the same prion protein (Bessen and Marsh, 1992, 1994). This suggested that prion strains were the result of conformational heterogeneity; a model that bypassed the need for a nucleic acid genome.

Despite this study and increasing evidence from others, there remained resistance to not only the protein-only prion hypothesis, but also to the possibility that prion strains result from distinct infectious conformations of the prion protein. How could a protein fold into multiple stable conformations? How is the information encoding these distinct conformations accurately propagated to new hosts? The answers to these questions and consensus on the protein-only hypothesis could not be satisfied without a glimpse into the structures of these infectious particles, as explained by Robertson when he stated that "Final judgment about the nature of the scrapie agent will not be possible until the structures of the prion protein and any associated nucleic acid can be related to scrapie strain specificity" (Robertson et al., 1985). Thus, structural insights into prion particles were not only a matter of curiosity, rather, they held the possible solution to the prion strain enigma as well as bore some of the burden of proof for the protein-only hypothesis.

Since the protein-only hypothesis was first introduced in 1982, much progress has been made in the structural characterization of these proteinaceous infectious particles, often providing answers, or at worst, more tangible models for the existence of prion strains. Prions adopt elongated, fibrous structures that result from the templated polymerization of the prion protein (Cohen and Prusiner, 1998). The ultrastructural characteristics, tinctorial properties, and templating mechanism of prion aggregation

closely mirrors that of other amyloids, and as such has followed a similar trajectory of structure elucidation (Maji et al., 2009). Although the first indications that prion strains relied on aggregate conformation were made over 15 years ago, high resolution insight into different conformations of prion aggregates and a detailed molecular understanding of the consequences of these structural deviations on prions strain phenotypes has only recently arisen.

One of the primary difficulties with studying mammalian prion strain structures is isolating appropriate particles that represent the true infectious material. A given prion strain aggregate may not represent a single infectious conformation, rather, it may be composed of a spectrum of structures, not all of which may act as a true templating and toxic aggregate. Selectively extracting structural data from strain-specific toxic aggregates has thus been difficult and limited to largely qualitative conformational studies. Following Bessen and Marsh's initial observations of the Dy and HY strains in TME, further work demonstrated the same conformational link to strains in Human prion diseases. This study used a transgenic mouse line harboring a chimeric human/mouse Prp. When infectious prion material was isolated from different sporadic and familial Creutzfeld-Jakob disease (sCJD and fCJD respectively) patients and inoculated into this transgenic mouse background, distinct strain phenotypes were observed in these otherwise genetically identical mice (Safar et al., 1998; Telling et al., 1996). Furthermore, like Bessen and Marsh, infectious material from mice infected with different prion strains displayed different protease sensitivities. Further work on *in vivo* prion aggregates lead to the development of a few techniques aimed at identifying conformational differences between strains. The first employed the use of antibody

detection. Here, antibodies specific for Prp recognized their substrate most efficiently when the antigen was unfolded. Thus, different strains of prions with different conformations had correspondingly different accessibilities for antibody binding (Safar et al., 1998). Another method utilized protease sensitivity and aggregate unfolding in guanidine hydrochloride (GdnHCl). Here, aggregate unfolding in increasing concentrations of GdnHCl was monitored through a concomitant increase in protease sensitivity. Thus, half-maximal denaturation concentrations of several prion aggregates from different *in vivo* strains were determined, demonstrating a high degree of variation between strains, but reproducibility within the same strain (Peretz et al., 2001). Both of these techniques were again able to identify the presence of reproducible conformation diversity between prion strains, however, they lacked the resolution to see what the conformational difference might be.

Higher resolution studies of mammalian prion strains have been more successful in a "synthetic" setting using *in vitro* formed recombinant protein aggregates. By using purely *in vitro* systems, achieving a more homogeneous aggregate population may be more successful, however, perhaps at the expense of studying a truly physiologically relevant species. For example, recombinant Prp lacks the native glycophosphatidylinositol (GPI) anchor and branched sugars, and producing infectious material from a purely *in vitro* source has been met with low infectious titers (May et al., 2004). Despite these caveats, multiple conformations of amyloid-like fibers have been produced from recombinant Prp. Unlike *in vivo* prion sources which relied on different isolates of infectious matter, multiple conformations formed *in vitro* by either modulating the form of agitation while spontaneous fiber polymerization occurred (rotation vs.

shaking) (Makarava and Baskakov, 2008), or by seeding prion monomers from one animal species (i.e. mouse Prp), with two different animal species (i.e. Syrian hamster and Human Prp) (Jones and Surewicz, 2005). Both these approaches yielded distinct conformations of aggregates that appeared morphologically different by either EM or AFM, and displayed differing β-sheet content by FTIR. Whether these same conformational differences could be observed in physiologically relevant aggregates, however, remains to be seen.

A more recent structural study aimed to combine *in vivo* prion aggregates and recombinant Prp protein to make *in vitro* aggregates that more closely reflect the *in vivo* structures (Smirnovas et al., 2009). This approach is based on a technique developed by Soto and co-workers called protein misfolding cyclic amplification (PMCA), where brain extracts from prion diseased animals are used as seed to convert non-diseased brain homogenates, thus amplifying the infectious material (Castilla et al., 2005; Saborio et al., 2001). Through repeated dilutions and amplifications, one can dilute out most of the original infectious seed, leaving primarily amplified infectious material. The recent work from Surewicz's group similarly used PMCA by starting with infected hamster brain, and used it to seed *e. coli*-produced Prp. H/D exchange-MS performed on these PMCA aggregates and spontaneously formed aggregates again produced distinct structures, with the PMCA aggregates having an extended amyloid fold. Although these observed structural heterogeneities may not represent aggregates of two distinct strains of prions, they do provide an idea of what strain-specific conformational differences may look like, and demonstrate the ability to do high-resolution structural studies on aggregates that may more closely resemble true infectious particles. It will be exciting to see if this

technique could be extended to using multiple strains of *in vivo* aggregates as seeds for recombinant protein and what conformational differences between these strains emerge.

Although progress has been made in demonstrating that distinct prion strains arise from distinct conformations of the prion aggregates, a complete and fully satisfying link between conformation and phenotypic diversity has yet to be established in mammalian systems. As mentioned, this is largely due to the difficulty of isolating a homogeneous preparation of physiologically relevant aggregates that are amenable to structural studies. Luckily, a more amenable analogous prion system in yeast exists, and is where much of the recent progress towards understanding the relationship between aggregate conformation and phenotype has been made.

Although prions were first hypothesized as the infectious agent for a class of diseases known collectively as transmissible spongiform encephalopathies (TSEs), they were later proposed to be the underlying causative agent for a number of epigenetic traits in fungi (Wickner, 1994; Wickner et al., 2007). The yeast [*PSI*] system has provided an ideal platform on which to study the conformational basis of prion strain variants. The [*PSI*] prion state can be monitored through a convenient color-based phenotypic readout wherein [*psi*$^-$] (non-prion) cells adopt a red color phenotype, and [*PSI*$^+$] (prion) cells have a white color phenotype (Chien et al., 2004). [*PSI*$^+$] strains are manifested in the form of different shades of color, ranging from dark pink, to pink, to white, and these color phenotypes remain stable upon multiple passages (Derkatch et al., 1996). Precise control over which prion strain is adopted was demonstrated for two strains named Sc4 (white) and Sc37 (pink) (King and Diaz-Avalos, 2004; Tanaka et al., 2004). When recombinant Sup35p (the causative prion protein for [*PSI*$^+$]) was polymerized into aggregates at two

different temperatures, 4°C and 37°C, the resulting aggregates conferred the Sc4 and Sc37 [*PSI*$^{+}$] strains respectively when introduced into [*psi*$^{-}$] yeast. Due to the loss-of-(Sup35p)function nature of the [*PSI*$^{+}$] prion, the actual differences in color phenotypes could be explained by differing residual quantities of soluble, and therefore functional, Sup35p in the [*PSI*$^{+}$] backgrounds. What could influence the levels of unaggregated protein in these cells? Chapter 2 describes a biophysical study that began to shed light on this, showing that the two fiber preparations differed in their physical characteristics such as breakability and fiber polymerization rate; two factors that could have substantial effects on the efficacy of aggregates to recruit and sequester functional protein into the non-functional and aggregated state.

The second question this thesis aimed to address is, what are the conformational differences between the aggregates responsible for different prions strains? A number of studies have employed various different techniques in an effort to determine the structure of SupNM fibers as well as the conformational differences between the different strains. Cysteine mutants with coupled EPR probes is an approach used by our lab to map the presence of structured at a particular residue through EPR probe mobility at that location (Tanaka et al., 2004; Tanaka et al., 2005). This approach gave a low-resolution picture of fiber structure that spanned from residue 8 through 117. Conformational differences between the Sc4 and Sc37 strains were subtle, most significant around residue 46 (Tanaka et al., 2005). FTIR in this study, however, provided some insight into the size of the core structures, as Sc4 had slightly less β-sheet content than Sc37 (Tanaka et al., 2005). This was consistent with biophysical data that suggested the Sc4 fibers were a weaker conformation than Sc37 (Tanaka et al., 2004; Tanaka et al., 2006). These data

suggested different size amyloid core structures between the two conformations. Another study that utilized cysteine mutants but coupled with fluorescent probes provided a different structural viewpoint (Krishnan and Lindquist, 2005). This study identified the core amyloid fold to be between residues 25 and 106. Furthermore, they identified a "head" region (residues 25-38) and "tail" region (residues 91-106) which they argue participate in a "head to head" and "tail to tail" fiber assembly process. Strains in this study differed again by different size amyloid cores, Sc4 having a smaller one, and the precise locations of the "head" and "tail" contacts.

Another approach aimed to elucidate SupNM fiber structure and strain differences was x-ray crystallography. David Eisenberg's group has been successful at getting a number of short (5-7 residues) peptides from a number of amyloidogenic proteins including Sup35 to form microcrystals (Nelson et al., 2005; Sawaya et al., 2007; Wiltzius et al., 2009). When they solved the structures of these crystals, they found them to be in an amyloid-like arrangement. Thus, this potentially provided an atomic-resolution view of amyloid, and Sup35, fiber structure. The Sup35 peptide structure consisted of the sequence GNNQQNY derived from residues 7-13. This structure showed the peptide in an in-register parallel β-sheet structure with two sheets facing each other face to face, their respective side chains interdigitating with each other forming a sort of "steric zipper" structure. This steric zipper was found to be a tight interface devoid of any water molecules, suggesting that a perturbation such as a mutation with conjugated probe inserted into this area would likely disrupt the local structure (Nelson et al., 2005).

The previously described structural studies have all had their limitations. They either had very low resolution (FTIR), had limited resolution and relied on a potentially

perturbative technique (cysteine mutants with probes), or utilized a short peptide that may reflect a completely different structure outside of the context of the other 246 residues. Chapter 3 describes our study that aimed to circumvent these limitations through the use of hydrogen/deuterium (H/D) exchange NMR. Here I describe that Sc4 exhibited extremely stable structure from residues 8-37 while Sc37 was structured from residues 5-70. This represents an almost doubling of structure in the Sc37 conformation, with evidence that the region of overlapping structure (residues 8-37) represented distinct conformations. Thus, Sc4 and Sc37 most likely form two different folds on the monomeric level, rather than having an identical "amyloid core" with the Sc37 displaying an expansion of structure beyond that core. Although we provide evidence and mechanism for the existence of strains in this particular yeast prion, much more work is needed to get to a similar level of understanding in the far more difficult mammalian prion system.

Chapter 2

The Physical Basis of How Prion Conformations Determine Strain Phenotypes

The Physical Basis of How Prion Conformations Determine Strain Phenotypes

Motomasa Tanaka[2,3], Sean R. Collins[1], Brandon H. Toyama[1] & Jonathan S. Weissman[1]

[1]*Howard Hughes Medical Institute, Department of Cellular and Molecular Pharmacology, University of California-San Francisco and California Institute for Quantitative Biomedical Research, San Francisco, California 94143, USA*

[2]*PRESTO, Japan Science and Technology Agency, 4-1-8 Honcho Kawaguchi, Saitama 332-0012, Japan*

[3]*RIKEN Brain Science Institute, Hirosawa2-1, Wako, Saitama351-0198, Japan*

Abstract

A principle that has emerged from studies of protein aggregation is that proteins typically can misfold into a range of different aggregated forms. Moreover, the phenotypic and pathological consequences of protein aggregation depend critically on the specific misfolded form (Caughey and Lansbury, 2003; Dobson, 2003). A striking example of this is the prion strain phenomenon, in which prion particles composed of the same protein cause distinct heritable states (Collinge, 2001). Accumulating evidence from yeast prions such as [*PSI*$^+$] and mammalian prions argues that differences in the prion conformation underlie prion strain variants (Brachmann et al., 2005; Collinge, 2001; King and Diaz-Avalos, 2004; Legname et al., 2004; Tanaka et al., 2004). Nonetheless, it remains poorly understood why changes in the conformation of misfolded proteins alter their physiological effects. Here we present and experimentally validate an analytical model describing how [*PSI*$^+$] strain phenotypes arise from the dynamic interaction among the effects of prion dilution, competition for a limited pool of soluble protein, and conformation-dependent differences in prion growth and division rates. Analysis of three distinct prion conformations of yeast Sup35 (the [*PSI*$^+$] protein determinant) and their in vivo phenotypes reveals that the Sup35 amyloid causing the strongest phenotype surprisingly shows the slowest growth. This slow growth, however, is more than compensated for by an increased brittleness that promotes prion division. The propensity of aggregates to undergo breakage, thereby generating new seeds, probably represents a key determinant of their physiological impact for both infectious (prion) and non-infectious amyloids.

The [*PSI*$^+$] phenotype results from self-propagating beta-sheet-rich aggregates (amyloid) of the yeast Sup35 translation termination factor (Shorter and Lindquist, 2005; Tuite and Koloteva-Levin, 2004; Wickner, 1994). Inactivation of Sup35 causes a nonsense suppression phenotype in [*PSI*$^+$] yeast that can be readily monitored using an ade1 nonsense reporter gene. [*psi*$^-$] colonies require adenine and accumulate a red pigment, whereas [*PSI*$^+$] exhibits a range of heritable strain variants that vary from dark pink to white depending on the degree of Sup35 inactivation (Derkatch et al., 1996; Kochneva-Pervukhova et al., 2001). Recently, it has been possible to create synthetic prion forms of Sup35 in vitro that have adopted distinct infectious (prion) conformations, which when introduced into yeast lead to different prion strain phenotypes (King and Diaz-Avalos, 2004; Tanaka et al., 2004). This ability to create distinct amyloid conformations of Sup35 in vitro, and to monitor their in vivo consequences makes [*PSI*$^+$] a uniquely powerful system for investigating what has become a central problem in the field: how do differences in the physical properties of conformationally different misfolded forms modulate their physiological effects?

To pursue this question, we first developed an analytical model that allows us to predict how changes in the physical properties of the Sup35 prion alter observable in vivo features of [*PSI*$^+$] such as the fraction of aggregated protein (that is, colour phenotype) and the size and number of the Sup35 aggregates. This effort relies on a number of elegant studies that revealed that prion propagation involves two mechanistically distinct and potentially strain-dependent steps (Bradley et al., 2002; Castilla et al., 2005; Cox et

al., 2003; Krishnan and Lindquist, 2005; Kryndushkin et al., 2003; Kushnirov and Ter-Avanesyan, 1998; Shorter and Lindquist, 2005; Tuite and Koloteva-Levin, 2004): a growth phase in which unconverted protein adds onto existing prion particles, and a division phase that generates new prion particles. [PSI^{+}] growth results from the self-propagating nature of amyloid fibres, whereas division is mediated by the host chaperone machinery, principally by the Hsp104 chaperone (Cox et al., 2003; Shorter and Lindquist, 2005). The rate of Sup35 fibre growth is linearly proportional to both the concentrations of soluble Sup35 and prion fibres in vitro. Moreover, fibre growth can occur after translation and independently of Hsp104 in vivo (Collins et al., 2004; Satpute-Krishnan and Serio, 2005; Shorter and Lindquist, 2005), and both in vitro (DePace and Weissman, 2002) and in vivo (Ness et al., 2002) (see also Supplementary Data for details), minimal fibre depolymerization occurs on the timescale of cell division. We therefore modelled fibre growth as a second order irreversible process with a rate constant (β) that varies depending on the specific prion strain. The rate of prion replication is proportional to the mass of polymerized Sup35 and this rate of division (γ) may depend on the prion strain conformation (Kryndushkin et al., 2003; Shorter and Lindquist, 2005). With these considerations in mind, and also accounting for the synthesis of new Sup35 and the dilution of all components through cellular growth, we obtained a set of differential equations that describe the time evolution of the concentration of soluble Sup35 ([x]), aggregated Sup35 ([z]) and prion particles ([y]) in terms of rate constants for translation (α), fibre growth (β), fibre division (γ) and cellular growth (R) (Fig. 2.1a). One feature not specifically included in this model is lateral association of fibres, as this is expected to have a minimal effect on the underlying processes of fibre growth and division,

although lateral association will decrease mitotic stability by reducing the number of independently heritable elements ('propagons') (see Supplementary Data for a more complete discussion).

An important aspect of this analysis, which extends upon previous efforts to model prion dynamics (Hall and Edskes, 2004; Masel et al., 1999; Weissmann, 2004), is that it accounts for the existence of distinct stable prion strains even under equilibrium conditions. Specifically, these equations yield two steady-state solutions, one corresponding to a [*psi*$^-$] state and another to a [*PSI*$^+$] state (Fig. 2.1a). The nature of the [*PSI*$^+$] solution varies with both β and γ, allowing us to predict how the colour phenotype and number of prion fibres depend on the underlying fibre properties (Fig. 2.1b). The [*PSI*$^+$] solution is non-negative (and hence physically relevant) only for sufficiently great fibre growth and division rates ($\beta\gamma > R^3/\alpha$), but in these cases it is mathematically stable: perturbations altering the concentration of fibres or soluble Sup35 levels are corrected by restoring forces that bring these concentrations back to their steady-state levels. The existence of a continuum of stable steady-state solutions parameterized by the conformation-dependent properties β and γ accounts for how it is possible, even in dividing cells, to have a broad range of prion strains with differing levels of soluble prion protein and characteristic numbers of fibres (Derkatch et al., 1996; Kochneva-Pervukhova et al., 2001; Weissmann, 2004) (Fig. 2.1b). Interestingly, the [*psi*$^-$] solution is not stable and thus is able to persist only because of the extremely high kinetic barrier to *de novo* prion formation. The kinetic instability of the [*psi*$^-$] state helps explain the high efficiency of transmission of [*PSI*$^+$] because, as we confirm by examining the

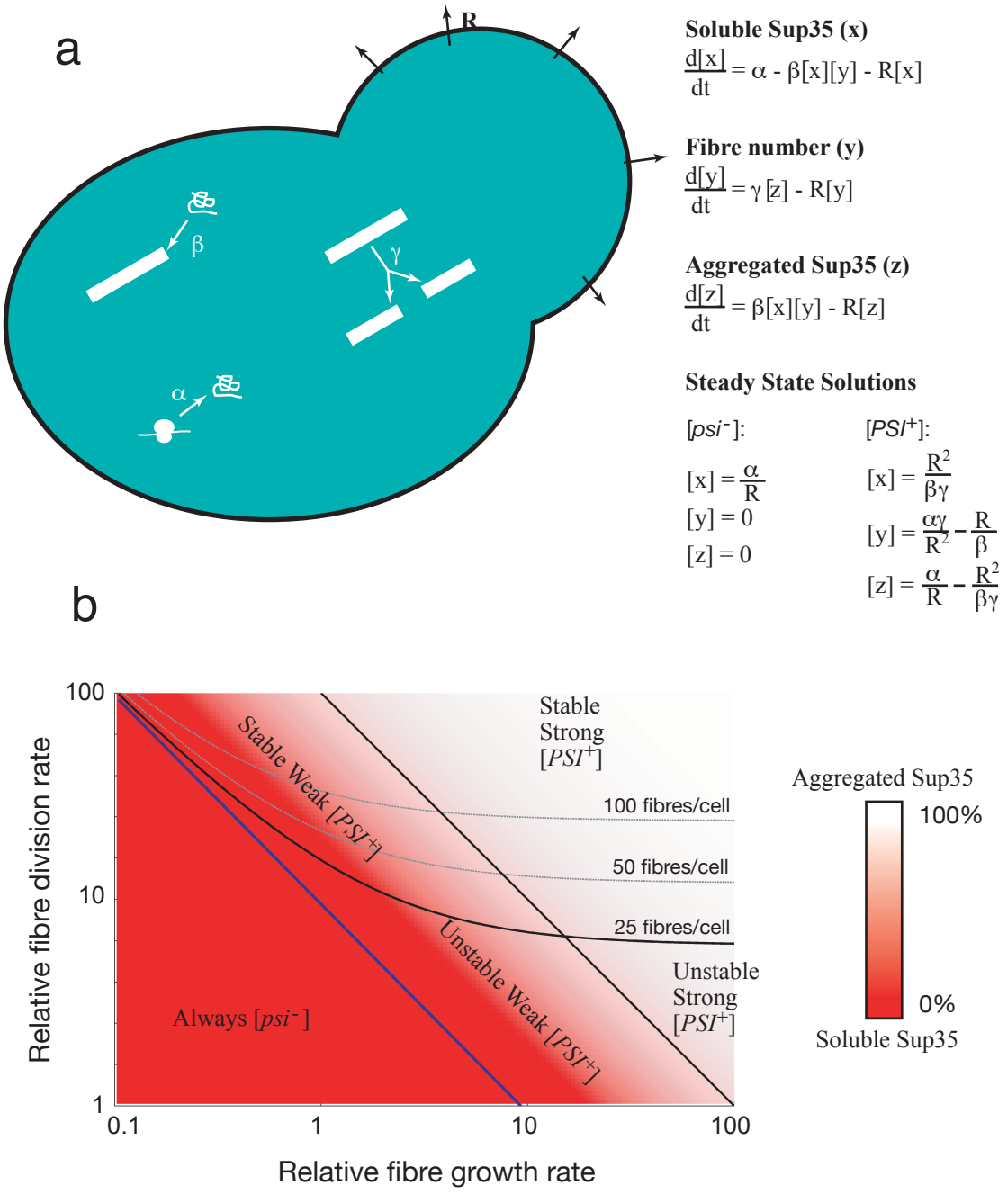

Figure 2.1 An analytical model describing prion strains

a, Left: graphical representation of parameters defining prion dynamics. α, β, γ and R are the rate constants for translation of Sup35, fibre growth, fibre division and growth of yeast cells, respectively. Right: differential equations describing time-dependent changes in concentration of soluble Sup35 monomer [x], Sup35 fibre [y] and aggregated Sup35 [z]. The two steady-state solutions representing [*psi*⁻] and [*PSI*⁺] states are defined by the equations shown. b, Graphical representation of the effect of growth and division rates on strain phenotypes. Aggregation states of Sup35 are represented by a colour gradient. Curved lines demark states that have the same number of fibres per cell. The blue line represents a threshold below which stable prion propagation is not possible. Black lines illustrate borders between [*PSI*⁺] states showing strong or weak colour phenotypes or large (stable) versus small (unstable) numbers of fibres per cell, as indicated.

concentration dependence of the efficiency of prion infectivity (Fig. 2.5), introduction of a single prion particle can convert [*psi*$^-$] yeast into [*PSI*$^+$]. Finally, extension of our analysis to explore the phenomenon of strain competition, which occurs when two different conformations are introduced into a cell, indicates that, as previously noted (Bradley et al., 2002), the prion strain with the lowest levels of soluble protein (highest $\beta\gamma$ value) is dominant.

We next used our ability to create in vitro three distinct infectious conformations of the prion-forming domain (Sup-NM; residues 1–254) of Sup35 to investigate experimentally how changes in the physical properties of an aggregate dictate its resulting in vivo strain phenotypes. These three amyloid forms, termed Sc4, Sc37 and SCS, are generated by spontaneously polymerizing Sup-NM at 4 °C or 37 °C, or by seeding polymerization of *Saccharomyces cerevisiae* Sup-NM with seeds derived from the highly divergent *Candida albicans* Sup35 homologue, respectively (Tanaka et al., 2005). Previous studies demonstrated that Sc4, Sc37 and SCS amyloids have well-defined localized conformational differences that can be robustly propagated in vivo (Krishnan and Lindquist, 2005; Tanaka et al., 2004; Tanaka et al., 2005). Moreover, infection of [*psi*$^-$] yeast with the Sc4, Sc37 and SCS Sup-NM amyloids leads to readily distinguishable prion strains termed [*PSI*$^+$(Sc4)], [*PSI*$^+$(Sc37)] and [*PSI*$^+$(SCS)] that qualitatively show strong (white), intermediate (pink) and weak (dark pink) colour phenotypes, respectively (Fig. 2.6).

We measured the intrinsic fibre growth rate (β) for these distinct strain conformations of Sup-NM amyloid using an atomic force microscopy (AFM)-based single-fibre growth assay (DePace and Weissman, 2002) (Fig. 2.2a–c). At physiological temperatures (room temperature and above), the Sc4 fibres showed the slowest growth (109 nm) compared with Sc37 (511 nm) and SCS (261 nm) fibres. Intriguingly, the relative growth rate of Sc4 fibres increases significantly at low temperature (4 °C) (Fig. 2.2a). Comparison of histograms of fibre growth measurements at the different temperatures reveals that the three conformations have minimally overlapping distributions, arguing strongly that Sc4, Sc37 and SCS fibres represent distinct and conformationally pure forms. We confirmed the slow fibre growth rate of Sc4 amyloid by a bulk seeding assay in the presence of 25% Ficoll, which mimics the macromolecular crowding effects found in cells (Fig. 2.2d). Thus, we conclude that the Sc4 fibre form shows the slowest intrinsic growth rate (~30% relative to Sc37 in crowding conditions) despite the fact that it leads to the strongest strain phenotype.

Examination of the physical strength of the different prion conformations suggests a solution to this paradox: the slower growth of Sc4 amyloid is accompanied by a marked increase in the propensity of these fibres to be fragmented. We measured the frangibility of the different Sup-NM amyloid conformations in vitro by forming long (> 1 microm) Sup-NM amyloids in the absence of shear forces and then subjecting them to fragmentation by stirring the solution with a magnetic stir bar. AFM analysis revealed that this treatment shattered Sc4 amyloids into many tiny fibres (< 100 nm) but had a relatively modest effect on Sc37 and SCS fibres (Fig. 2.3a and Fig. 2.7). Concurrent with

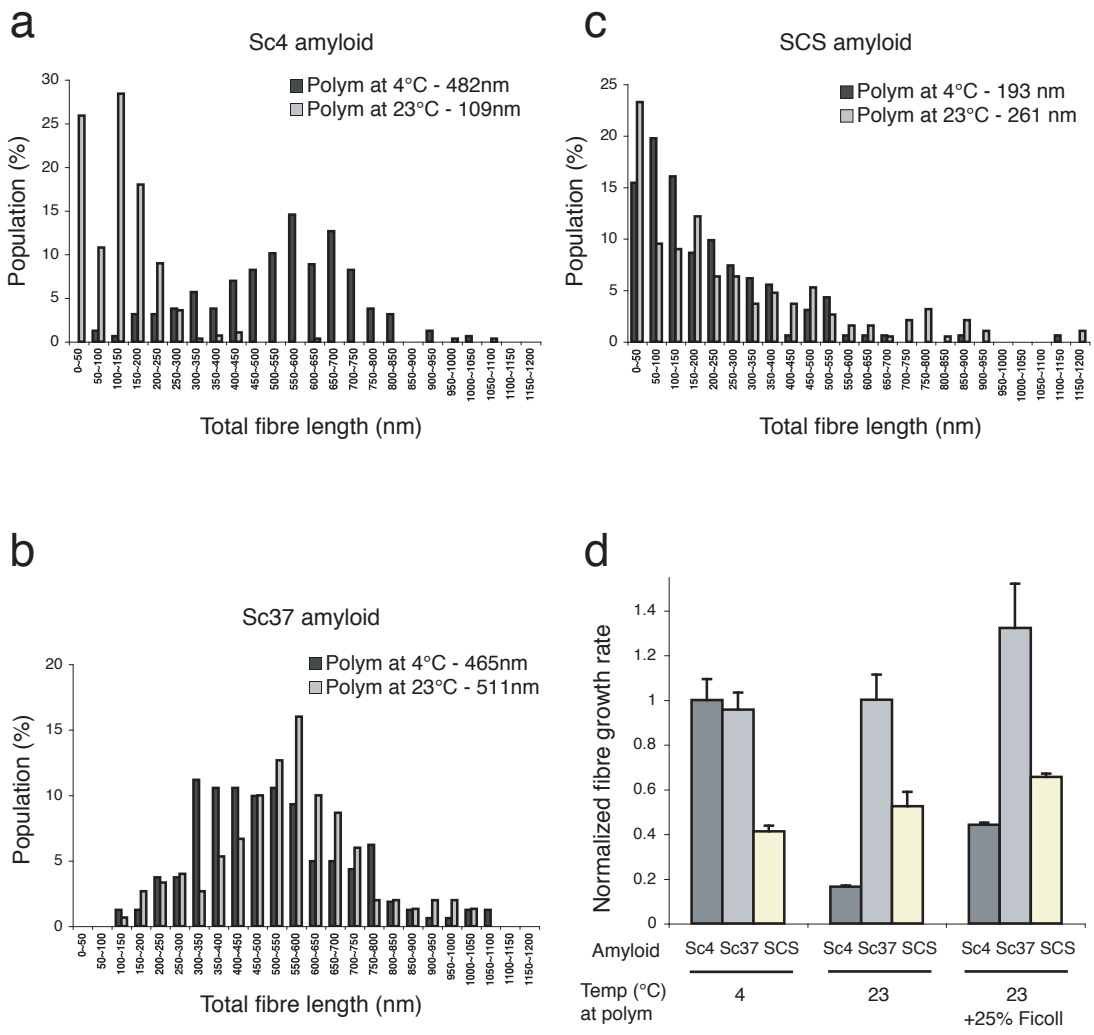

Figure 2.2 Effects of strain conformation on fibre growth rate

a–c, Growth distribution for (a) Sc4, (b) Sc37 and (c) SCS amyloids at 4 °C (black) and 23 °C (grey) (distribution at 37 °C was similar to that at 23 °C, data not shown). Fibre growth rates were determined by an AFM-based single fibre assay. The values indicate mean total fibre length grown over 10 min at 2.5 M soluble Sup-NM. d, Bulk measurements of the relative growth rate of Sc4, Sc37 and SCS Sup-NM amyloids. Polymerization of Sup-NM with indicated fibre seeds was performed at 4°C or 23°C in the absence or presence of 25% (wt/wt) Ficoll and the rate of addition of Sup-NM monomers was monitored by thioflavin T fluorescence. The fibre growth rates of each Sup-NM amyloid conformation were normalized with the AFM-based mean length of the corresponding fibres at 4 °C. Values are expressed as mean s.d

the appearance of new fibre ends, we observed a marked increase in seeding efficacy and prion infectivity for the Sc4 fibres but not the Sc37 or SCS fibres (Fig. 2.3b, c). The increase in fragility of the Sc4 fibres is consistent with their increased sensitivity to denaturants and proteases relative to Sc37 and SCS fibres (Krishnan and Lindquist, 2005; Tanaka et al., 2004; Tanaka et al., 2005) and probably results from strain-specific structural differences in inter molecular contacts and a shorter, less stable amyloid core (Krishnan and Lindquist, 2005; Tanaka et al., 2005).

We next examined whether Sc4 also shows an increased rate of division under physiological conditions in intact cells, using an elegant approach developed previously (Cox et al., 2003; Ness et al., 2002). Specifically, the rate at which the equilibrium prion state is restored after transient growth in guanidine hydrochloride (Gdn-HCl)-containing media, which reversibly inhibits Hsp104 (and thus prion division) (Ferreira et al., 2001; Jung and Masison, 2001), reports on the product of the intrinsic propensity of fibres to be divided per unit length (γ) and the growth rate (β) (see Fig. 2.8). The [*PSI*$^+$(Sc4)] strain regenerated the equilibrium prion state after removal of Gdn-HCl substantially more rapidly than [*PSI*$^+$(Sc37)], which itself was faster than the [*PSI*$^+$(SCS)] strain (Fig. 2.3d). Thus, the slow growth rate (low beta) relative to Sc37 fibre amyloid is more than overcome by the faster in vivo prion division rate for the Sc4 but not the SCS strain.

We used a range of assays to define the in vivo phenotypes of the [*PSI*$^+$(Sc4)], [*PSI*$^+$(Sc37)] and [*PSI*$^+$(SCS)] strains. Subjecting extracts to high-speed centrifugation revealed that, as would be expected from its weak colour phenotype, the [*PSI*$^+$(SCS)]

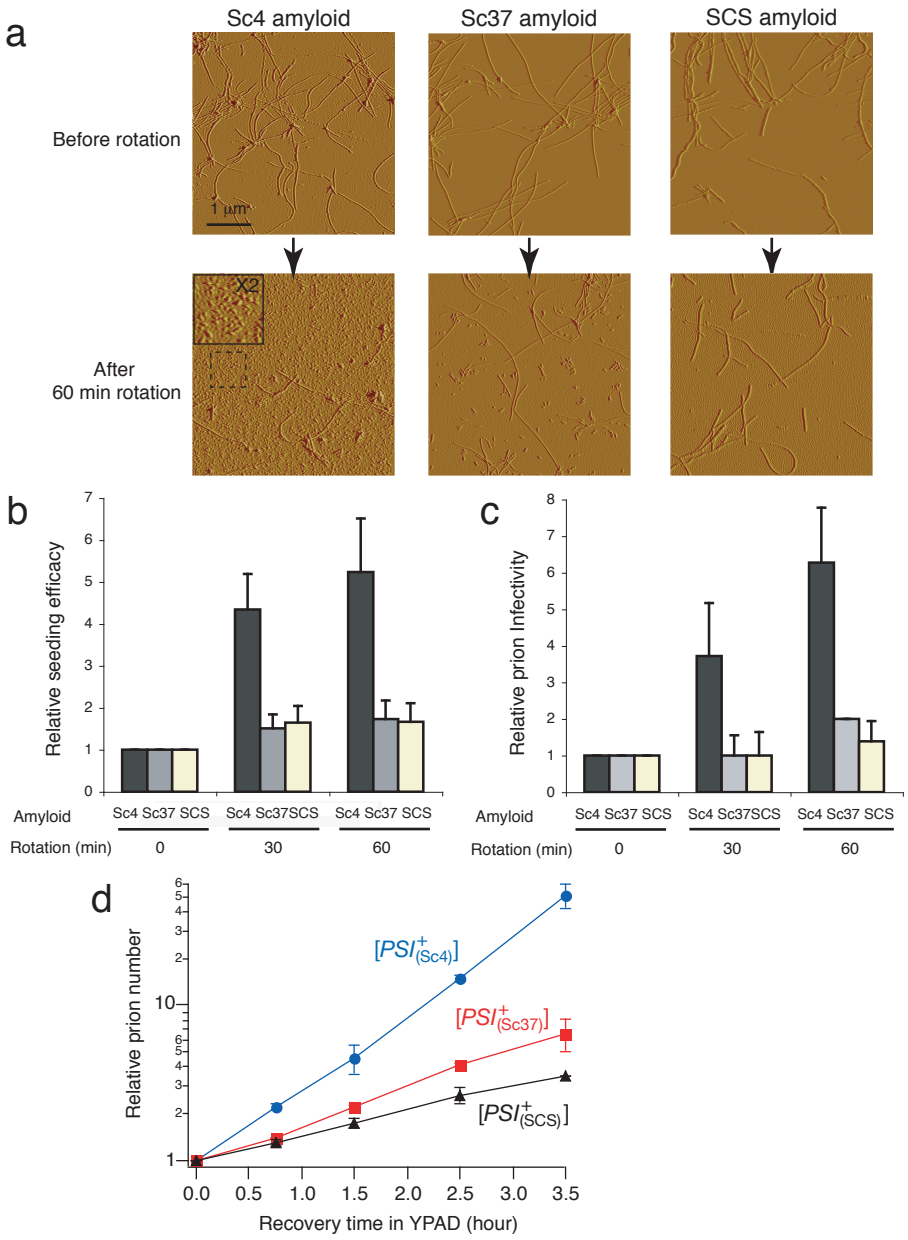

Figure 2.3 Effects of strain conformation on fiber fragmentation

a, Typical AFM images of Sc4 (left), Sc37 (middle) and SCS (right) Sup-NM amyloids before (top) and after (bottom) stirring for 60 min. Prior to stirring, for all three conformations, most fibres are long (> 1 m). After stirring, more than 98% of Sc4 amyloids are <100 nm whereas more than 60% of both Sc37 and SCS amyloids are >100 nm (see Supplementary Fig. S3). A magnified view (black box) of small fibre fragments (dotted box) is also shown for Sc4 fibres. b, Relative seeding efficacy of Sc4, Sc37 and SCS Sup-NM fibres before and after stirring for 30 or 60 min. c, Relative prion infection efficiency of Sc4, Sc37 and SCS Sup-NM fibres (1 M Sup-NM monomer) before and after rotation for 30 or 60 min. d, Effects of strain conformation on prion growth and division in vivo. Rate of generation of equilibrium prion state after Gdn-HCl treatment as a function of recovery time for [*PSI*$^{+}$(Sc4)], [*PSI*$^{+}$(Sc37)] and [*PSI*$^{+}$(SCS)] strains. The doubling times of the prions are 37 +/- 2, 79 +/- 10 and 116 +/- 1 min for [*PSI*$^{+}$(Sc4)], [*PSI*$^{+}$(Sc37)] and [*PSI*$^{+}$(SCS)] strains, respectively, which correspond to relative values of 3, 1 and 0.67 (see Fig. 2.8 for details). Values are expressed as mean s.d.

strain contains a substantial pool of soluble Sup35, compared to a modest one for [*PSI*$^+$(Sc37)] and a barely detectable one for [*PSI*$^+$(Sc4)] (Fig. 2.4a). In contrast, examination of prion number and size by several independent assays indicated that, as expected by its relative fragility, [*PSI*$^+$(Sc4)] is distinguished from the other two strains by having a large number of relatively small prion elements. A 'propagon counting' assay (Cox et al., 2003) (see also Supplementary Data for details) indicated that the apparent number of propagons per cell in the [*PSI*$^+$(Sc4)] strain was much larger (129 +/- 21) than that found in either [*PSI*$^+$(Sc37)] (20 +/- 9) or [*PSI*$^+$(SCS)] (26 +/- 5) (Fig. 2.4b). Furthermore, both agarose gel analysis in the presence of SDS (Fig. 2.4c), which is thought to report on the length of individual prion fibres15, and sedimentation of prion particles in non-denaturing conditions (Fig. 2.9), established that the prion particles in the [*PSI*$^+$(Sc4)] strain are smaller than those found in either [*PSI*$^+$(Sc37)] or [*PSI*$^+$(SCS)] strains.

As illustrated in Fig. 2.4d, the above strain phenotypes are in excellent agreement with those predicted by our analysis based on their observed prion growth and division properties. In particular, the slow growth of SCS amyloids (~30–50% relative to Sc37), which is not accompanied by an increase in division rate, accounts for the observed increase in the level of soluble Sup35 and the correspondingly weaker colour phenotype. In contrast, although Sc4 also grows more slowly than Sc37, this is over-ridden by a much higher division rate ($\beta\gamma$ is estimated to increase ~3-fold, see Supplementary Data for details), leading to a decrease in the amount of soluble Sup35 (that is, white colour

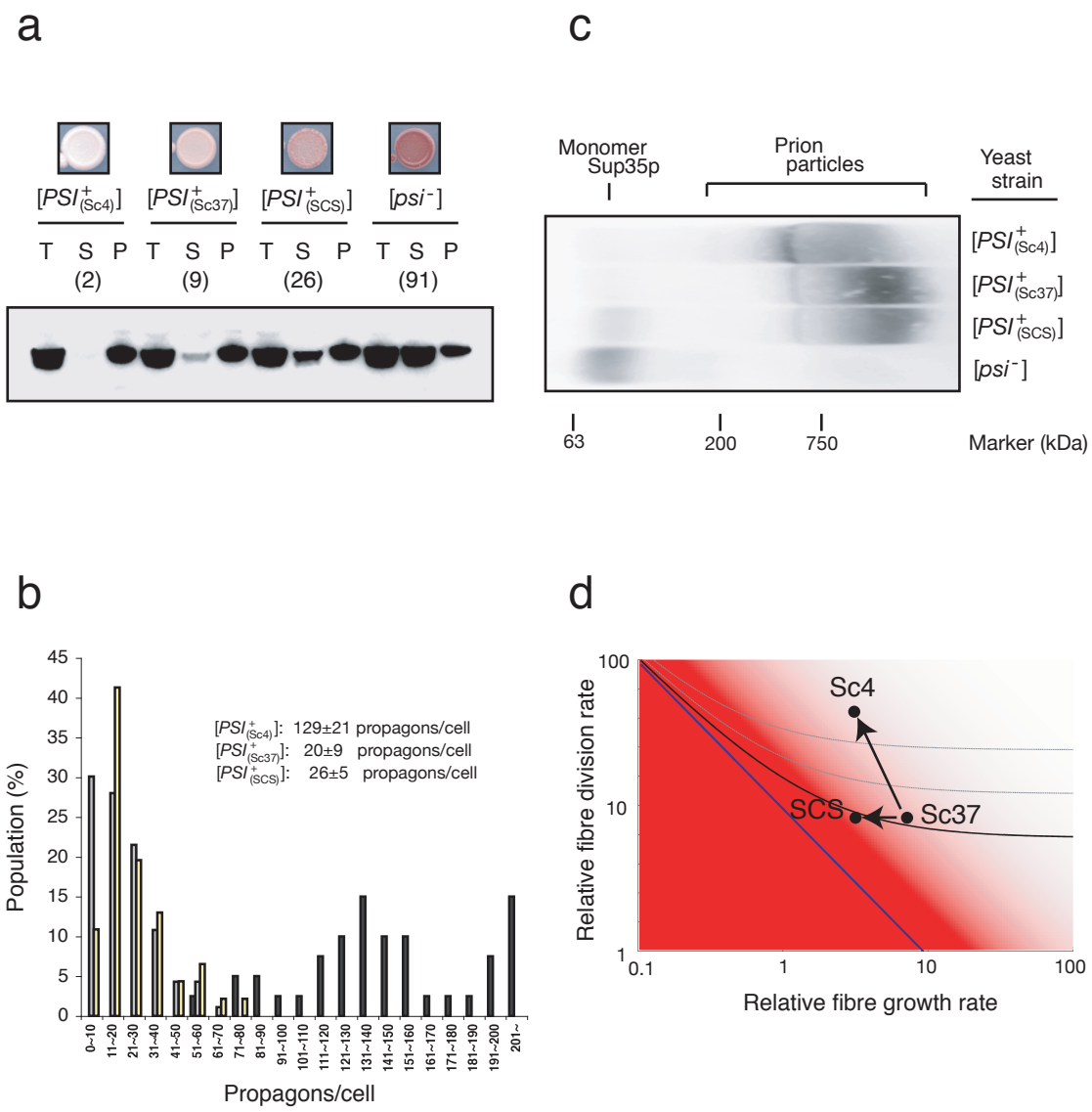

Figure 2.4 Analysis of distinct [*PSI*$^+$] strain phenotypes

a, Sedimentation analysis of strains by ultracentrifugation. Total (T), supernatant (S) and pellet (P) fractions of yeast extracts of the indicated strains were analysed by SDS–PAGE followed by western blotting using a polyclonal anti-Sup-NM antibody. Shown in parenthesis are the mean band intensities of supernatant fractions, relative to that of total fractions (100). Typical colour phenotypes of [*PSI*$^+$(Sc4)], [*PSI*$^+$(Sc37)], [*PSI*$^+$(SCS)] and [*psi*$^-$] strains are shown in the top panels. b, Frequency of propagon numbers per cell for [*PSI*$^+$(Sc4)] (black), [*PSI*$^+$(Sc37)] (grey) and [*PSI*$^+$(SCS)] (yellow) strains. (See also Supplementary Information.) c, Agarose gel analysis of prion particle size in lysates of [*PSI*$^+$(Sc4)], [*PSI*$^+$(Sc37)], [*PSI*$^+$(SCS)] and [psi-] strains. Migration positions of prion particles and monomeric Sup35 are indicated. d, Strain phenotypes predicted by our model (Fig. 1b) based on the observed growth and division properties of the various [*PSI*$^+$] strains. SCS and Sc4 both show decreased growth rates (30–50%) compared with Sc37. In the case of SCS, this is not accompanied by an increase in division rate and thus leads to the observed increase in soluble Sup35. In contrast, for Sc4 the large increase in the division rate offsets the slow growth (increases 300% relative to Sc37), leading to a decreased pool of Sup35 and an even more dramatic increase in propagon number (decrease in size). As in Fig. 1b, the calculated amount of soluble Sup35 is shown with a red–white scale

phenotype) and an even more dramatic increase in the number (and thus decrease in size) of fibres.

Our work establishes the critical role of the frangibility of a prion aggregate in dictating the strength of its strain phenotype. Less is known for other systems about the mechanism of amyloid growth and division. Nonetheless, similar dynamic effects, with dilution mediated by proteolysis and clearance rather than cell division in post-mitotic cells, probably apply for other aggregation phenomena including both infectious (prion) and non-infectious amyloids(Hall and Edskes, 2004; Masel et al., 1999; Weissmann, 2004). Indeed, recent studies indicate that smaller aggregates of the mammalian prion protein PrP, which should be more readily generated by strains that form fragile particles, are markedly more infectious than larger aggregates (Silveira et al., 2005). Additionally, for synthetic mammalian prions, the incubation time increases as the physical stability of the prion increases (G. Legname, H. O. Nguyen, D. Peretz, F. E. Cohen, S. J. DeArmond and S. B. Prusiner, personal communication). Finally, it has been observed that stronger [*PSI*$^+$] strains typically have shorter fibres in vivo than weaker strains (Kryndushkin et al., 2003), although the physical properties of the prions (for example, their propensity to be fragmented) were not examined. Taken together, these considerations argue that variability in the brittleness of aggregates represents a major mechanism by which prion conformations dictate the strength of strain phenotypes. Thus, a strong impediment to the production of highly infectious synthetic mammalian prions may be the propensity to generate highly stable amyloid forms in vitro (Castilla et al., 2005; Legname et al., 2004). Conversely, therapeutic efforts to minimize the impact of protein aggregation could be

tailored not only to slow aggregate formation and growth but also to decrease the rate of fragmentation either by increasing fibre stability or inhibiting chaperone machinery. More broadly, this analysis allows for a unified analytical treatment of both non-infectious and infectious (prion) amyloids with prion states arising only when the rate of amyloid growth, division and spread is sufficient to allow sustained propagation.

Methods

Yeast strains and fibre preparation

We used isogenic [*psi*$^-$][*RNQ*$^+$] and [*PSI*$^+$] derivatives of the 74D-694 yeast strain (Santoso et al., 2000). [*PSI*$^+$(Sc4)], [*PSI*$^+$(Sc37)] and [*PSI*$^+$(SCS)] strains were made by infection of [*psi*$^-$] yeast with in-vitro-produced Sup-NM Sc4, Sc37 and SCS amyloids (Tanaka et al., 2005). Sc4, Sc37 and SCS (previously termed as Sc[Ca3[Sc4]]) fibres were produced as described previously (Tanaka et al., 2005), using bacterially produced pure Sup-NM proteins carboxy-terminally tagged with 7x histidine (Tanaka et al., 2004).

In vitro analysis of strain conformations of Sup-NM amyloids

The AFM-based single-fibre assay was performed as reported previously (DePace and Weissman, 2002) with some modification. Each histogram involved the measurement of at least 150 individual fibres. The fibre growth rate of distinct Sup-NM amyloid fibres was also examined by thioflavin T fluorescence (Tanaka et al., 2005), in the absence or presence of Ficoll PM70 to the final concentration of 25% (wt/v). For fibre rigidity assay, Sup-NM amyloids were formed by polymerizing Sup-NM (5 μM) in a beaker (2.2 cm diameter), containing 2 ml of 5 mM potassium phosphate buffer containing 150 mM

NaCl (pH 7.4), overnight under undisturbed conditions in the presence of 5% (mol/mol) seed of Sc4, Sc37 and SCS amyloids at 4, 37 and 23 °C, respectively. The amyloid solution was stirred by a magnetic stir bar (3 mm diameter, 1 cm length) at ~100 r.p.m. and an aliquot was taken at 0, 30 and 60 min and used for morphological, seeding efficacy (Tanaka et al., 2005) and prion infectivity (Tanaka et al., 2004) analyses. The detailed methods are described in Supplementary Data.

In vivo analysis of prion strains

The curing assay of [*PSI*$^{+}$] with Gdn-HCl was followed by a previously developed procedure (Cox et al., 2003; Ness et al., 2002). The propagon counting experiment was performed as described previously18. For agarose gel analysis, yeast cell lysates were prepared with glass beads, and prion particles in the lysates were separated by horizontal 1.6% agarose gels in TAE buffer containing 0.1% SDS (Kryndushkin et al., 2003), followed by immunoblotting with a polyclonal anti-Sup-NM antibody (Santoso et al., 2000). Sedimentation analysis was performed as reported previously (Tanaka et al., 2004) with some modification. The detailed methods are described in Supplementary Data.

Acknowledgements

We thank G. Legname and S. Prusiner for communicating their results before publication, B. Cox and T. Serio for personal communication, and T. C. Keller III for providing us with chicken pectoralis extracts. We also thank C. Cunningham, J. Newman, L. Osherovich, M. Schuldiner, K. Tipton and members of the Weissman laboratory for helpful discussion and critical reading of the manuscript. M.T. was partly supported by

JSPS and Uehara Memorial postdoctoral fellowships for research abroad. S.R.C. was supported by predoctoral fellowships from the Burroughs Wellcome Fund. Funding was also provided by the Howard Hughes Medical Institute, The David and Lucile Packard Foundation and the National Institutes of Health (J.S.W.). Author Contributions S.R.C. led the development of the analytical model. M.T. was responsible for the execution of the experiments, with the exception of the fibre growth studies, which were conducted by B.H.T. and M.T. M.T., S.R.C. and J.S.W. were primarily responsible for the design, interpretation and written description of the results.

Competing interests statement:

The authors declared no competing interests.

Supplementary information accompanies this paper.

Supplementary Methods

(1) Yeast strains and reagents

Throughout *in vivo* experiments, we used isogenic [*psi*$^-$][*RNQ*$^+$] and [*PSI*$^+$] derivatives of 74D-694 [MATa, *his3*, *leu2*, *trp1*, *ura3*; suppressible marker *ade1-14*(UGA)] (Santoso et al., 2000). [*PSI*$^+$(Sc4], [*PSI*$^+$(Sc37] and [*PSI*$^+$(SCS)] strains were made by infection of [*psi*$^-$] with *in vitro* produced Sup-NM Sc4, Sc37 and SCS amyloid fibres (Tanaka et al., 2005). Sc4, Sc37 and SCS (previously termed as Sc[Ca_3[Sc4]]) fibres were produced as described previously (Tanaka et al., 2005). Sup-NM proteins carboxy-terminally tagged

with 7x-histidine were expressed in *E. Coli*. (DE3) and purified as reported previously (Tanaka et al., 2004).

(2) *In vitro* analysis of strain conformations of Sup-NM amyloids

Sup-NM amyloid fibres were prepared by dilution of the denatured proteins into buffer A (5mM potassium phosphate buffer, 150mM NaCl, pH7.4) in the absence or presence of 5% (mol/mol) seed. Sup-NM SCS amyloid fibres were formed at 23°C with 5% (mol/mol) seed of SCS amyloids. The AFM-based single fibre assay was performed as reported previously (DePace and Weissman, 2002), with the exception that Sup-NM fibre seeds produced by spontaneous polymerization were directly used without passage through multiple rounds of polymerization and reseeding. Each histogram involved the measurement of at least 150 individual fibres. The fibre growth rate of distinct Sup-NM amyloid fibres was also examined by thioflavin T fluorescence, as reported previously (Tanaka et al., 2005), in the absence or presence of Ficoll PM70 (Amersham Biosciences) to the final concentration of 25% (wt/v). For fibre rigidity assay, Sup-NM amyloid fibres were formed by polymerizing Sup-NM (5μM) in a beaker (2.2cm diameter), containing 2ml of buffer A, overnight under undisturbed conditions in the presence of 5% (mol/mol) seed of Sc4, Sc37 and SCS amyloids at 4, 37 and 23 °C, respectively. The amyloid solution was stirred by a magnetic stir bar (3mm diameter, 1cm length) at ~100 rpm and an aliquot was taken at 0, 30, 60 min and used for morphological, seeding efficacy and prion infectivity analyses. Images of the Sup-NM fibres before and after the stirring were acquired by AFM (Digital Instruments, MultiMode AFM, Nanoscope software). Seeding

efficacy of the Sup-NM amyloids before and after the stirring was examined by thioflavin T fluorescence, as reported previously (Tanaka et al., 2005).

(3) *In vivo* analysis of prion strains

Protein infection experiments were performed as reported previously (Tanaka et al., 2004). The curing assay of [*PSI*$^+$] with guanidine hydrochloride (Gdn) was performed following the procedure by Cox, Tuite and coworkers (Cox et al., 2003; Ness et al., 2002). Logarithmic cultures of [*PSI*$^+$(Sc4)], [*PSI*$^+$(Sc37)] and [*PSI*$^+$(SCS)] strains were grown in YPAD+3mM Gdn for 12-15 hours, transferred to YPAD media and cultured for 0, 0.75, 1.5, 2.5 and 3.5 hours. The cultures were then returned to YPAD+3mM Gdn media and samples were taken at 2~4-hour intervals over ~30-40 hours. Percentage of [*PSI*$^+$] cells were determined by plating ~200 cells on 1/4 YEPD plates. The yeast generations were calculated using a hemocytometer and colony counts on 1/4 YEPD plates at each sample time. The percentages of [*PSI*$^+$] cells are normalized with that at the time when they were put into or returned to YPAD+3mM Gdn media and to 100% [*PSI*$^+$] cells at this time of rescue; the fraction of [*psi*$^-$] colonies that were in the culture at the time of rescue was subtracted from the percentage of [*psi*$^-$] colonies at each time point. Average numbers of prions per cell were determined by fitting the plot of percentage of [*PSI*$^+$] cells against cell generation with the equation, y=100*(1-exp(-A*(2^(-x)))), where x, y, and A indicates cell generation, percentage of [*PSI*$^+$] cells and an average number of prions, using IgorPro5.0 (WaveMetrics Inc.). The procedure of counting propagons was performed as described previously[5]. An aliquot of YEPD cultures of [*PSI*$^+$(Sc4)], [*PSI*$^+$(Sc37)] and [*PSI*$^+$(SCS)] strains was placed on YEPD+3mM Gdn plates and single

cells were transferred to different locations on the plate with a dissection microscope. Following ~30 hr of growth, a piece of agar containing whole individual colonies was resuspended with water and plated on SD-Ade or SD trace Ade (0.4 mg/L) plates. 1/4YEPD and YEPD+3mM Gdn plates were further used to distinguish [*PSI*$^+$] colonies from Ade$^+$ revertants. The number of [*PSI*$^+$] colonies was counted for more than 40 single cells for each [*PSI*$^+$] strain. The "jackpot" cells containing >200 propagons were excluded in calculation of the mean value. For agarose gel analysis, yeast cells were lysed in buffer (25mM Tris (pH7.5), 50mM KCl, 10mM $MgCl_2$, 1mM EDTA, 5% glycerol, 1mM PMSF, protease inhibitor cocktail (Roche)) with glass beads and the crude lysate was partially clarified by centrifugation at 10,000*g* for 5 minutes. The lysates (200μg) were treated with SDS sample buffer (50mM Tris (pH6.8), 5% glycerol, 2% SDS, 0.05% bromphenol blue) at 37°C for 10 minutes. The size of prion particles was analyzed by horizontal 1.6% agarose gels in TAE buffer containing 0.1% SDS (Kryndushkin et al., 2003), followed by immunoblotting with a polyclonal anti Sup-NM antibody (Santoso et al., 2000). Chicken pectoralis extracts including titin (3000 kDa), nebulin (750 kDa) and myosin heavy chain (200 kDa) as well as BenchMark Pre-Stained Protein Ladder (Invitrogen) were used to estimate molecular weight. Sedimentation analysis was performed as described previously (Tanaka et al., 2004), except for the speed and time of ultracentrifugation being 30,000 rpm and 10 minutes, respectively.

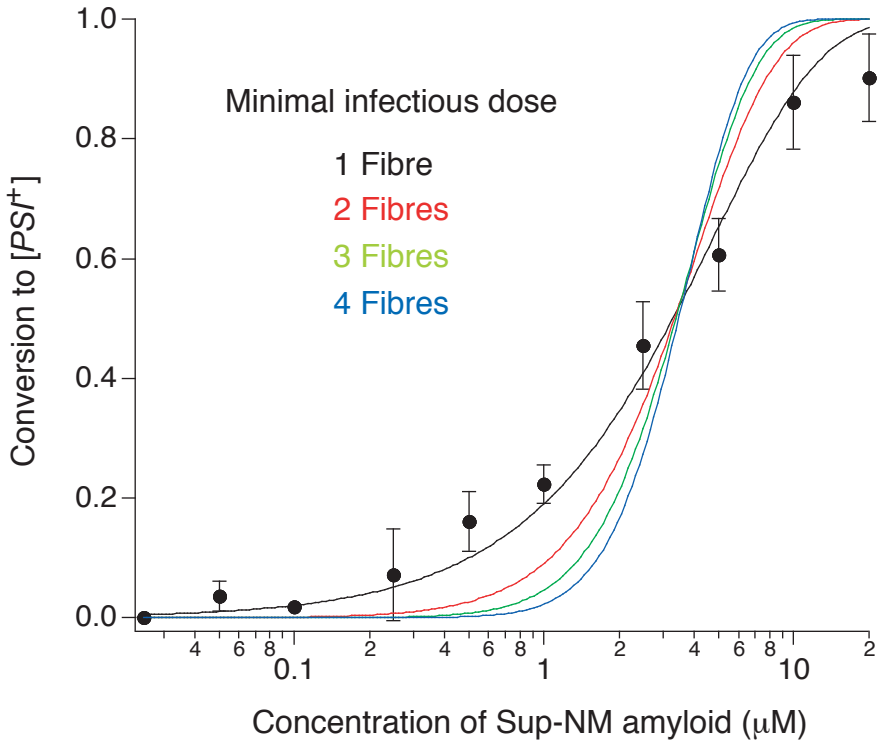

Fig 2.5 Introduction of a single prion fibre is sufficient to allow induction of a stable [*PSI*$^+$] state.

Shown is the efficiency of prion infectivity as a function of the concentration of Sup-NM amyloids (concentrations are given in terms of Sup-NM monomers) (Tanaka et al., 2004). Assuming that the number of introduced fibres is described by a Poisson distribution, the data are fitted to a model in which introduction of at least one (black), two (red), three (green) or four (blue) fibres is required to induce [*PSI*$^+$].

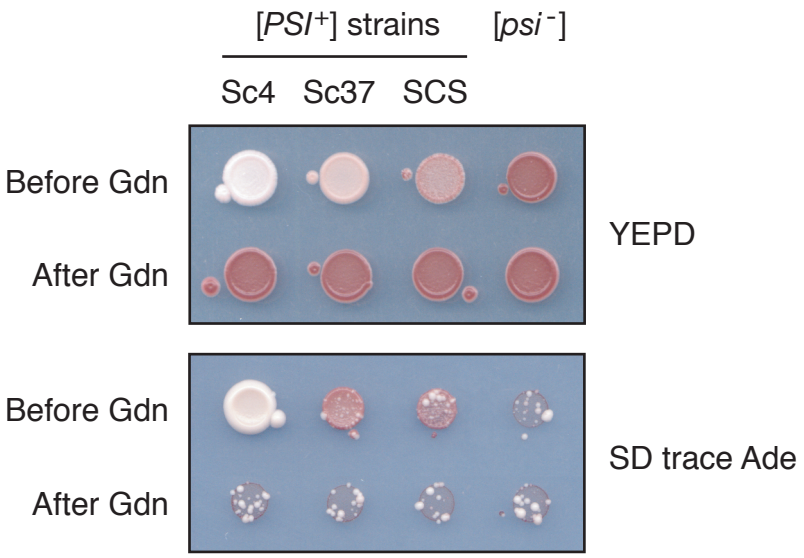

Figure 2.6 Ade1-14 read-through phenotype of typical [*PSI*$^+$] strains
Ade1-14 read-through phenotype of typical [*PSI*$^+$] strains produced by infection of [*psi*$^-$] with in vitro produced Sc4, Sc37 and SCS Sup-NM amyloid fibres as well as a [*psi*$^-$] control. The strains are grown on YEPD (top) and SD trace ADE (0.4 mg/L) (bottom) plates before and after passage on medium containing 3mM Gdn. Prion infectivities of the Sc4, Sc37 and SCS Sup-NM amyloid fibres (2.5mM) are 81±6, 38±6, and 24±7%, respectively.

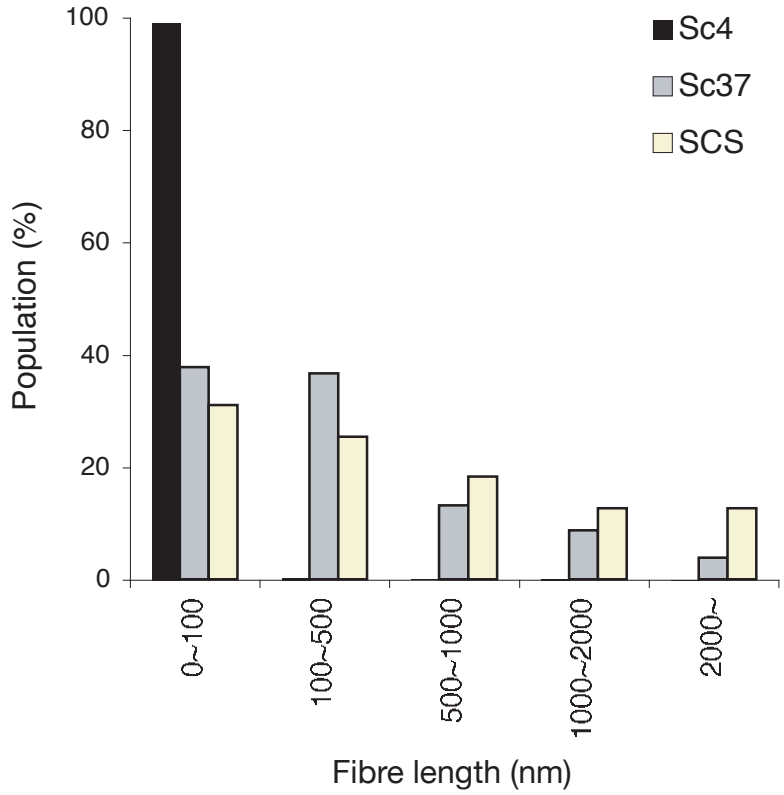

Figure 2.7 Frequency of Sup-NM fibre length after physical shearing of fibres for 60 minutes.

The histogram was made by measuring length of individual fibres from two thypical AFM images of Sc4 (black), Sc37 (gray) and SCS (yellow) Sup-NM fibres after stirring ofa magnetic bar for 60 minutes.

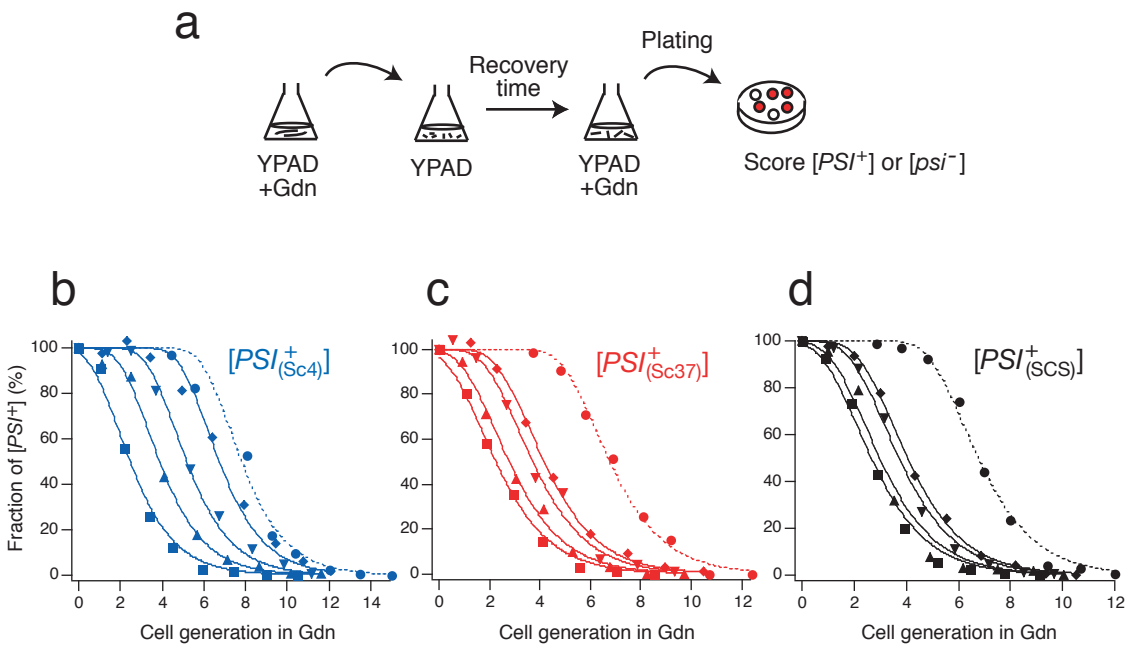

Figure 2.8 Effects of strains conformation on prion growth and division in vivo. (a) Schematic of experiment. Strains are cultured in YPAD+Gdn media until the prion state is nearly cured. Cultures are then transferred to normal YPAD media without Gdn, which restore prion division thereby allowing rescue of the prion state. After varying times, cultures are returned to YPAD+Gdn media and the extent to which the equilibrium prion state had been restored is determined by following the kinetics of prion curing. The rate at which the prion state is rescued during the YPAD growth step reports on the product of the growth and division rates (bg) (see also Supporting online text). (b,c,d) Kinetics of curing of (b) [*PSI*$^+$(Sc4)], (c) [*PSI*$^+$(Sc37)] and (d) [*PSI*$^+$(SCS)] strains during the final YPAD+Gdn growth step. The culture times in YPAD (i.e., rescue time) before returning to YPAD+Gdn media are 0.75 (square), 1.5 (triangle), 2.5 (inverted triangle) and 3.5 (diamond) hours. Also shown (circle) is the curing curve for yeast that did not receive the first Gdn treatment.

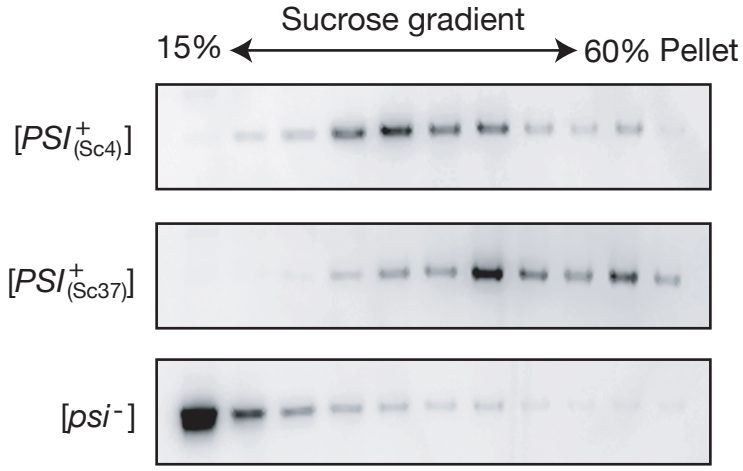

Figure 2.9 Separation of in vivo prion particles of distinct strains by sucrose gradient.

Prion particles in the lysates of [*PSI*$^{+}$(Sc4)], [*PSI*$^{+}$(Sc37)] and [*psi*$^{-}$] strains were separated by 15-60% sucrose cushion, followed by immunoblotting with a polyclonal anti Sup-NM antibody (Santoso et al., Cell, 100, 277-288, 2000). The lanes from left to right in the blot represent upper (15%) to bottom (60%) fractions of the sucrose gradient. The pellet fraction is shown on the far right lane in the blot. For the sucrose gradient experiment, yeast cells were lysed in buffer B (25mM Tris (pH7.5), 100mM NaCl, 10mM $MgCl_2$, 1mM DTT, 5% glycerol, 1mM EDTA, 1mM PMSF, protease inhibitor cocktail (Roche)) with glass beads. The crude lysate was partially clarified by centrifugation at 10,000g for 5 minutes. The supernatant (360mg) was layered upon 2mL of sequential 15%-40%-60% (wt/v) sucrose cushion in buffer B and ultracentrifuged at 33,000 rpm for 15 minutes (Beckman SW60 rotor). Fractions of 200mL were successively drawn from the top of the sucrose cushion. The pellet was resuspended with 200mL of 60% sucrose in buffer B. 10mL of each fraction was resolved by 4-12% SDS-PAGE, followed by immunoblotting with a polyclonal anti-Sup-NM antibody (Santoso et al., 2000).

Chapter 3

The structural basis of yeast prion strain variants

The structural basis of yeast prion strain variants

Brandon H. Toyama[1], Mark J. S. Kelly[2], John D. Gross[2], and Jonathan S. Weissman[1]

[1]Howard Hughes Medical Institute, Department of Cellular and Molecular Pharmacology,[2]Department of Pharmaceutical Chemistry, University of California-San Francisco and California Institute for Quantitative Biomedical Research, San Francisco, California 94158-2542, USA.

Abstract

Among the many surprises to arise from studies of prion biology, perhaps the most unexpected is the strain phenomenon whereby a single protein can misfold into structurally distinct, infectious states that cause distinguishable phenotypes (Cohen and Prusiner, 1998; Derkatch et al., 1996; Tuite and Cox, 2006). Similarly, proteins can adopt a spectrum of conformations in non-infectious diseases of protein folding; some are toxic and others are well tolerated (Chiti and Dobson, 2006). However, our understanding of the structural differences underlying prion strains and how these differences alter their physiological impact remains limited. Here we use a combination of solution NMR, amide hydrogen/deuterium (H/D) exchange and mutagenesis to study the structural differences between two strain conformations, termed Sc4 and Sc37 (ref. 5), of the yeast Sup35 prion. We find that these two strains have an overlapping amyloid core spanning most of the Gln/Asn-rich first 40 amino acids that is highly protected from H/D exchange and very sensitive to mutation. These features indicate that the cores are composed of tightly packed β-sheets possibly resembling 'steric zipper' structures revealed by X-ray crystallography of Sup35-derived peptides (Nelson et al., 2005; Sawaya et al., 2007). The stable structure is greatly expanded in the Sc37 conformation to encompass the first 70 amino acids, revealing why this strain shows increased fibre stability and decreased ability to undergo chaperone-mediated replication (Tanaka et al., 2006). Our findings establish that prion strains involve large-scale conformational differences and provide a structural basis for understanding a broad range of

functional studies, including how conformational changes alter the physiological impact of prion strains.

Sup35, the protein determinant of the yeast prion [*PSI*$^{+}$], is uniquely well suited to the analysis of the structural basis of prion strains (Tuite and Cox, 2006). Pure Sup35 spontaneously forms self-seeding, β-sheet-rich amyloid fibres in vitro (Glover et al., 1997). Introduction of these fibres into yeast causes stable conversion to the [*PSI*$^{+}$] state, thus establishing their infectious (prion) nature(Glover et al., 1997; King and Diaz-Avalos, 2004; Sparrer et al., 2000; Tanaka et al., 2004). Sup35 can adopt a variety of fibre conformations in vitro, which lead to clearly distinguishable prion strain variants when introduced into [*psi*$^{-}$] cells. For example, SupNM, a region of Sup35 encoding its prion function and composed of a Gln/Asn-rich N-terminal domain (N, amino-acid residues 1–123) and a highly charged middle domain (M, residues 124–253), can adopt distinct fibre conformations when polymerization is initiated at 4 °C and at 37 °C. Introduction of these conformations, termed Sc4 and Sc37, into yeast induces 'strong' and 'weak' in vivo prion strain phenotypes, respectively (Tanaka et al., 2004). Thus, the heritable differences in these strain variants are 'encoded' by the conformational differences between Sc4 and Sc37.

Although a battery of biophysical techniques have been employed to investigate Sup35 prion structures, no consensus view has emerged. One set of approaches introduced cysteine residues and inferred structure either by measuring side-chain reactivity or by incorporating biophysical probes such as paramagnetic spin labels or

pyrene fluorophores (Krishnan and Lindquist, 2005; Tanaka et al., 2004). One such study suggested that there is stable structure roughly comprising residues 31–86 and 21–121 for Sc4 and Sc37, respectively, with flanking sequences not being part of this amyloid core (Krishnan and Lindquist, 2005). Close intermolecular contacts between monomers seemed to be limited to short regions involving 'head-to-head' (residues 25–38) and 'tail-to-tail' (residues 91–106) interactions. An alternative view emerged from X-ray crystallography of the amyloid-like structure of the GNNQQNY peptide corresponding to residues 7–13 of Sup35 (ref. 6), a region outside the amyloid core suggested by the above study. Unlike the proposed head-to-head/tail-to-tail assembly, GNNQQNY formed extensive intermolecular contacts through in-register parallel beta-sheets that were stabilized by stacking side-chain amide hydrogen bonds between analogous asparagine and glutamine residues. Two sheets then came together face-to-face to form a water-free 'dry' interface in which opposing side chains interdigitated with each other, creating a compact 'steric zipper'. Caveats exist for both approaches: the X-ray crystallography analyses examined peptides outside the context of the prion domain, and the cysteine studies used side-chain modifications that might have perturbed the structure and stability of the fibres. Indeed, the extremely tight packing seen in the dry interfaces would probably be intolerant of side-chain alterations. More recently, solid-state NMR was used to probe for secondary structure in SupNM fibres in which a subset of amino acids were isotopically labeled (Shewmaker et al., 2006). Although it was not possible to obtain sequence-specific assignments, seven of eight leucine residues found in SupNM were suggested to form in-register beta-sheets. Because all except one leucine residue are in the M domain, it was proposed that much of the M domain was structured in the solid

state. This conclusion was surprising because the M domain is not absolutely required for prion function (Liu et al., 2002) and was thought to be largely disordered in fibres in solution (Krishnan and Lindquist, 2005; Tanaka et al., 2004). These conflicting perspectives emphasize the need for residue-specific structural information on full-length, unmodified SupNM fibres in solution.

We first examined SupNM fibre structure by solution NMR. Large complexes (that is, more than 100 kDa) are generally not amenable to solution NMR, as a result of line broadening, unless specialized spectroscopic techniques such as TROSY are employed (Fiaux et al., 2002). However, highly mobile regions within large complexes can sometimes be detected by using standard heteronuclear single-quantum coherence (HSQC) pulse sequences. Indeed, substantial portions of SupNM seem to be disordered in fibre forms, because ^{15}N-HSQC spectra from uniformly ^{15}N-labelled SupNM fibres revealed multiple robust peaks (Fig. 3.1a). To assess which regions of SupNM are flexible, we employed a strategy similar to that used in the solid-state NMR study and specifically ^{15}N-labelled the leucine residues. In dimethylsulphoxide (DMSO), in which SupNM is monomeric, seven of eight potential leucine peaks were observed, demonstrating the specificity of the labelling (Fig. 3.4). NMR spectra of ^{15}N-Leu-SupNM fibres contained at least four robust peaks with a smaller additional peak (Fig. 3.1b). Because all except one of the leucines are in the M domain (Fig. 3.1c), these data indicate that, in solution, large regions of the M domain remain highly mobile even in the fibre form, a view substantiated by the experiments below.

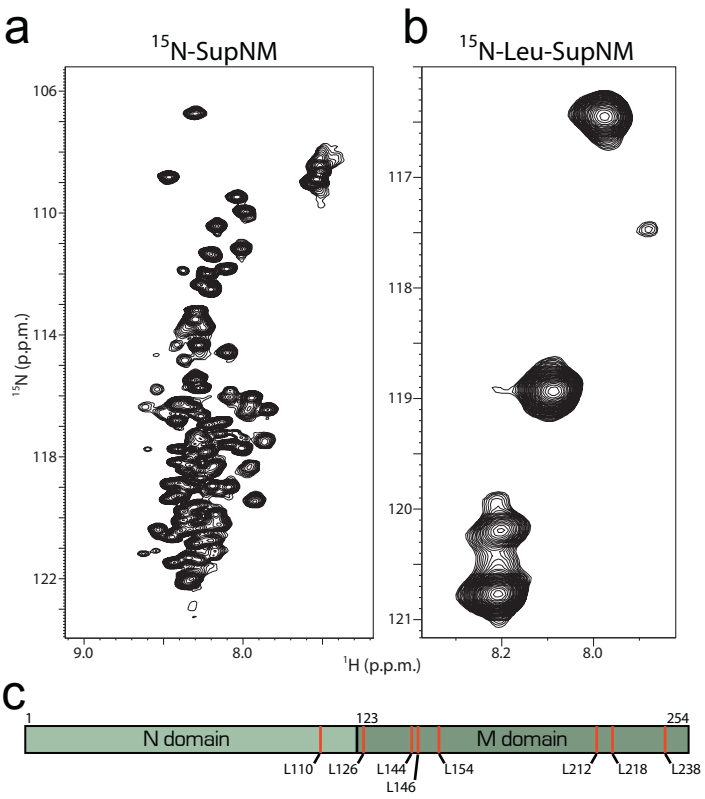

Figure 3.1 Solution NMR of SupNM fibers

a, ^{15}N-HSQC spectrum of uniformly ^{15}N-labelled SupNM fibres polymerized into the Sc4 conformation. b, ^{15}N-HSQC spectrum of SupNM Sc4 fibres specifically labelled with ^{15}N-leucine. c, Diagram showing the distribution of leucine residues in the SupNM sequence.

To obtain residue-specific information on the Sc4 and Sc37 conformations, we measured quenched hydrogen/deuterium (H/D) exchange by using NMR. H/D exchange is a sensitive probe of structure because hydrogen bonds inhibit the exchange of amide protons with water. We employed a recent protocol (Hoshino et al., 2002) that has enabled the structural analysis of a variety of amyloid fibres (Carulla et al., 2005; Hoshino et al., 2002; Luhrs et al., 2005; Ritter et al., 2005; Yamaguchi et al., 2004) by exploiting the ability of DMSO to dissolve fibres while preserving their exchange state. DMSO effectively dissolved SupNM fibres, yielding a well-dispersed ^{15}N-HSQC spectrum (Fig. 3.2a and Fig. 3.6a–c). However, assignment of the ^{15}N-HSQC, a prerequisite for measuring exchange, remained a challenge. SupNM is large (253 residues) compared with other amyloidogenic polypeptides studied (Carulla et al., 2005; Hoshino et al., 2002; Luhrs et al., 2005; Ritter et al., 2005), and the N domain has very low complexity; the first 40 residues (Sup1–40) are especially Gln/Asn-rich, and the adjacent residues 41–97 are composed of 5.5 imperfect oligopeptide repeats of the sequence PQGGYQQYN (Fig. 3.5). Through the use of more than 20 three-dimensional heteronuclear NMR experiments on 11 different uniformly and specifically labelled samples, we succeeded in assigning 163 of 215 visible peaks (Fig. 3.2a and Fig. 3.5) including assignments for 33 of the first 40 residues, several assignments in each oligopeptide repeat, and most of the M domain.

We monitored the extent of H/D exchange on uniformly ^{15}N-labelled Sc4 and Sc37 fibres at neutral pH at five time points ranging from 1 min to 1 week. Additionally, we performed H/D exchange for 1 day on Sc4 and Sc37 fibres specifically labelled with

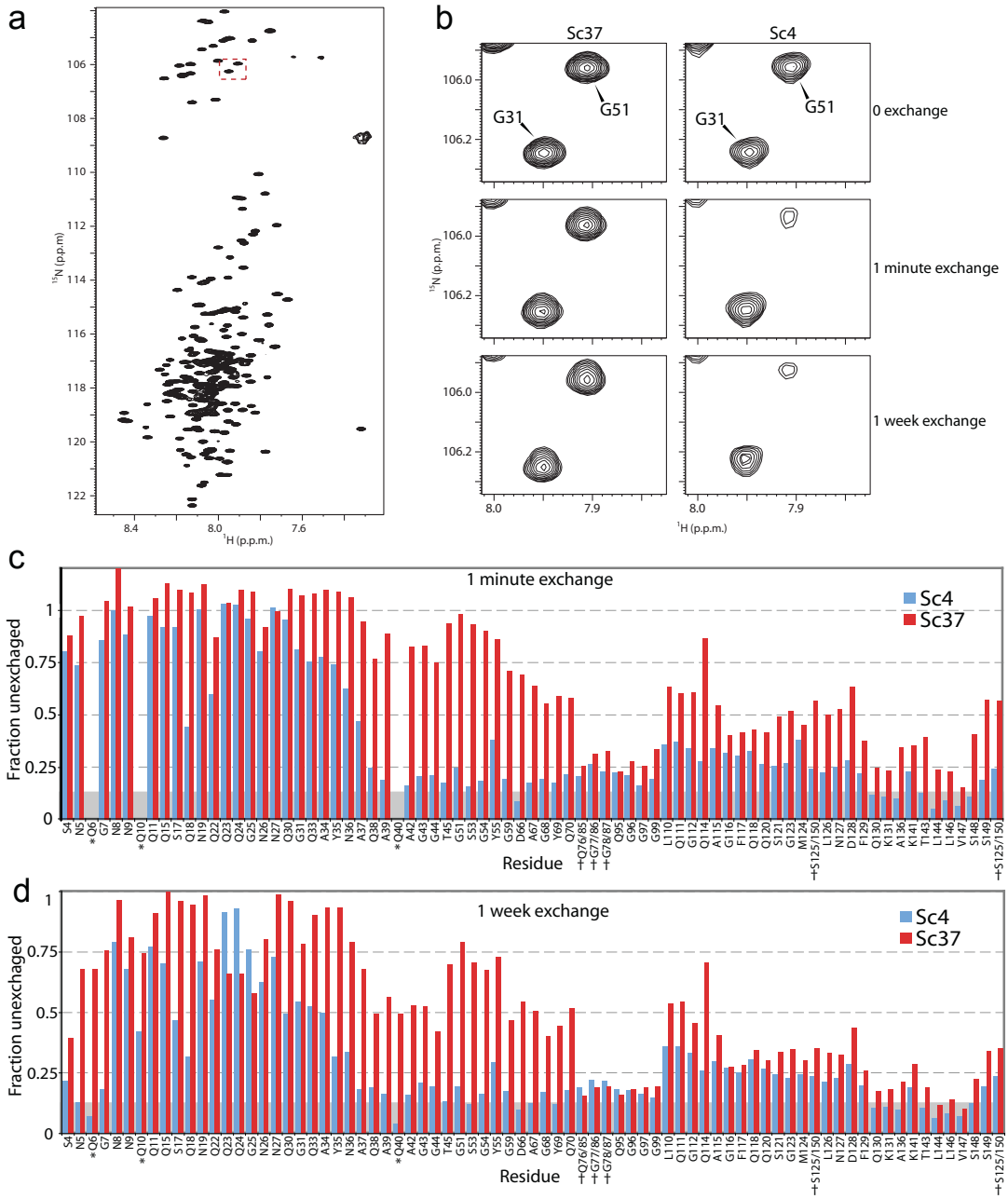

Figure 3.2 H/D exchange of Sc4 and Sc37 fibers

a, ^{15}N-HSQC spectrum of uniformly ^{15}N-labelled SupNM fibres dissolved in DMSO dissolution buffer. The red dashed box indicates residues shown in b. b, H/D exchange performed on the Sc4 and Sc37 conformations. ^{15}N-HSQC spectra for residues Gly 31 and Gly 51 (red dashed box in a) for the Sc37 (left panels) and Sc4 (right panels) conformations after 0 min (top panels), 1 min (middle panels) and 1 week (bottom panels) of exchange. c, d, Intensities for all assigned and unambiguous peaks as a fraction of the non-exchanged intensity after 1 min (c) and 1 week (d) of exchange on the Sc4 (blue) and Sc37 (red) conformations. Unassigned and ambiguous residues are not displayed. S4 and N5 in the Sc4 conformation have calculated protection factors of 6,478 (R^2 = 0.88) and 26,304 (R^2 = 0.93) respectively. Residues marked with an asterisk are resolved only in Glx specifically labelled H/D exchange experiments performed with a single 1-day exchange time point. Daggers indicate pairs of residues with overlapping peaks; values therefore represent the combined intensities. The grey bar represents the estimated minimum peak intensity.

^{15}N-Glu/Gln (Glx) to obtain data on key residues that had significant overlap in the uniformly labelled samples. Examination of the exchange spectra revealed multiple peaks that strongly resisted exchange in both conformation-independent and conformation-dependent manners (Fig. 3.2b–d). Three classes of exchange curves predominated (Fig. 3.6d). In the first class, amides completed exchange within 1 min, which corresponded to protection factors (the intrinsic rate of exchange divided by the observed rate) of less than 100. The second class showed only modest exchange even after 1 week, corresponding to highly stable regions with protection factors of at least 106. The third class of residues did not follow a single exponential: partial exchange was seen in the early time points, but the remaining fraction remained largely unexchanged by 1 week. Similar behaviour has been observed for other amyloid species (Luhrs et al., 2005; Yamaguchi et al., 2004) and may reflect multiple structural environments for these residues within the same fibre (see ref. 17).

Our data reveal overlapping core amyloid regions for Sc4 and Sc37 that encompass almost the entire Gln/Asn-rich Sup1–40 subdomain as well as a marked, strain-specific expansion of protected structure into the oligopeptide repeats in the Sc37 fibres (Fig. 3.2c, d). Both Sc4 and Sc37 conformations showed strong protection for residues 4–37, including the residues containing the GNNQQNY peptide, but had local differential protection patterns. In particular, adjacent residues 38–70, which encompass the first three oligopeptide repeats, showed high levels of protection in Sc37 but completed exchange within the first 1 min in Sc4. Both conformations seemed largely unprotected for residues 76–100, but significant protection was seen for some residues in

the 110–128 region. Most of the remaining M domain, including the leucine residues, showed modest protection (residues 150–231 in Fig. 3.7), which is consistent with the solution NMR results.

To test these findings independently, we probed for fibre secondary structure by introducing proline residues throughout SupNM to interfere with beta-sheet formation. Analysis of the conformation-specific effects of mutations on fibre formation poses a challenge because Sup35 can adopt multiple amyloid conformations. Hence, mutations detrimental to one fibre form can drive the formation of an alternative conformation rather than preventing fibre polymerization altogether (Chien et al., 2003). To circumvent this problem, we monitored the initial rate at which mutant monomers add to the end of preformed wild-type Sc4 and Sc37 fibres by using assays based on thioflavinT (thioT) and atomic force microscopy (AFM) (Chien et al., 2003; DePace and Weissman, 2002). These measurements directly assess the ability of each conformation to accommodate the mutation (Fig. 3.3a), thereby yielding conformation-specific structural information (Fig. 3.3b). We analysed a series of 36 individual SupNM proline mutations with locations chosen to overlap with and extend the H/D exchange data (Fig. 3.5). Of these mutations, 16 lie in Sup1–40, another 16 lie in the subsequent 41–100 oligopeptide region, and the last four target residues 101–150. Because the oligopeptide repeats were a major source of missing assignments, two corresponding Gln residues near the centre of each repeat were individually mutated to proline.

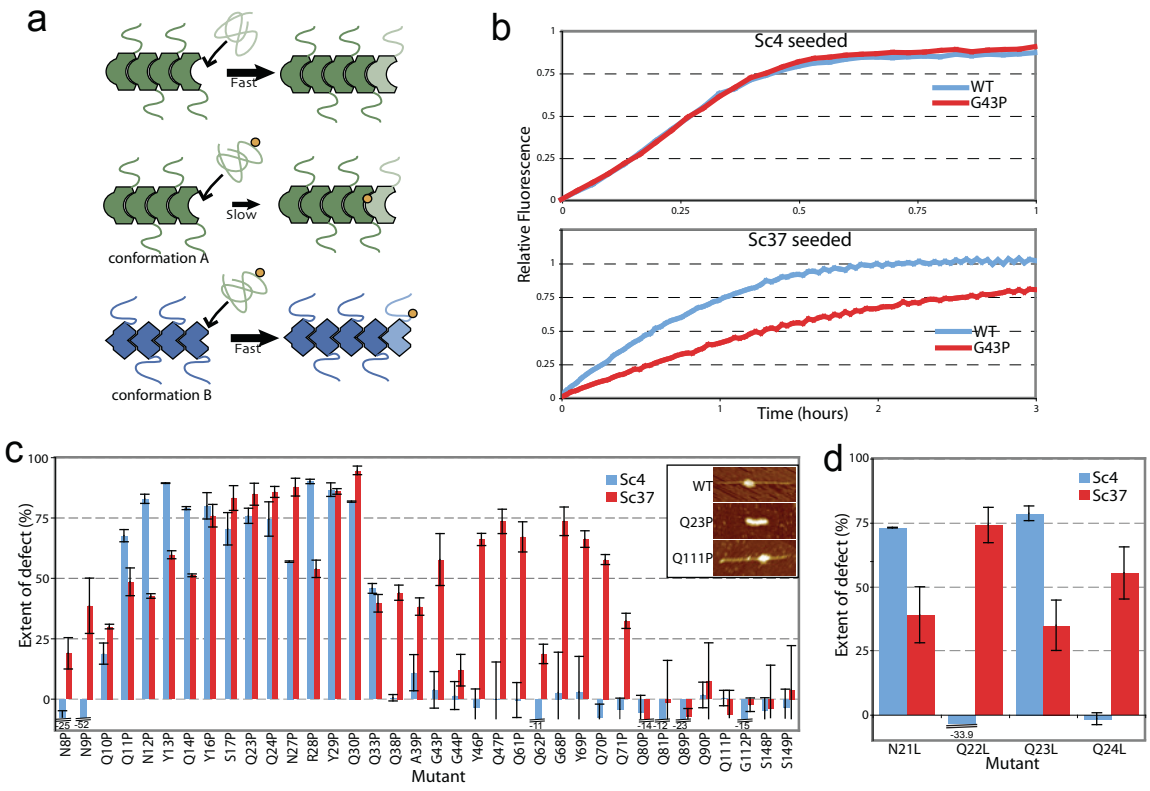

Figure 3.3 Mutational analysis of SupNM fibers

a, Diagram of the rationale for analysing the initial rate of polymerization. Here, the introduction of mutations (indicated by the circle) in regions important for fibre structure in conformation A but not in conformation B result in a slow initial rate of polymerization in a conformation-specific manner. b, Effect of proline mutants on polymerization as monitored by increase in thioT fluorescence. Wild-type Sc4 (upper panel) and Sc37 (lower panel) seeds were added to monomeric wild-type SupNM (blue curves) and SupNM G43P (red curves) and fibre polymerization was monitored by thioT fluorescence. Data were normalized to initial and final intensities. c, Effect of proline mutations on initial rates of polymerization of the Sc4 (blue) and Sc37 (red) conformations. ThioT polymerization assay was performed as described above for all mutants indicated. Data were normalized to initial and final intensities, initial time points were fitted to a line, and the slope (initial rate) was calculated. Values are the percentage by which each indicated mutant's initial rate deviated from the rate of wild-type polymerization, calculated as 100 (1 - Kmut/Kwt). Error bars indicate s.d. for two or three independent replicates. The inset shows representative pictures of indicated proline mutant growth (thin region) from wild-type (WT) Sc4 seed (thick region) revealed by AFM. d, The effect of leucine mutations on initial rates was measured as described above for the indicated leucine mutants of the Sc4 (blue) and Sc37 (red) conformations. Error bars indicate s.d. for two or three independent replicates.

The proline mutant analysis showed remarkable agreement with the H/D exchange data. With the exception of the termini, residues within the Sup1–40 subdomain were highly sensitive to mutations for both Sc4 and Sc37 seeds (Fig. 3.3c). AFM directly confirmed that proline mutations in this region profoundly inhibited the ability of mutant monomers to add to the ends of wild-type fibres (Fig. 3.3c inset, and Fig. 3.8a). In contrast, mutations within the first three oligopeptide repeats affected growth from Sc37 but not Sc4 seeds, whereas mutations from the fourth repeat up to the M domain had modest effects on growth for either conformation (Fig. 3.3c).

We extended this mutational analysis to probe tertiary structural contacts, focusing on the NQQQ sequence (residues 21–24) in the centre of the amyloid core. To minimize secondary structure perturbations, residues were individually changed to leucine, which has a similar beta-sheet propensity to that of both asparagine and glutamine. Leucine also has a higher intrinsic aggregation propensity (Chiti and Dobson, 2006) and is isosteric to asparagine. Despite the modest nature of the change, we saw strong inhibitory effects of leucine mutations for both Sc4 and Sc37 fibres (Fig. 3.3d and Fig. 3.8b). This indicates a critical role for the Asn/Gln side chains in stabilizing the amyloid core, possibly through interstrand hydrogen bonds and face-to-face interactions between beta-sheets such as those seen in the GNNQQNY peptide structure. Interestingly, Sc4 but not Sc37 displayed an alternating pattern of sensitivity to leucines, possibly indicative of a beta-sheet structure with one face buried and the other accessible in Sc4, but with both faces buried in Sc37 (Fig. 3.3d). Our data, in conjunction with those from earlier analyses (Nelson et al., 2005; Ross et al., 2005; Sawaya et al., 2007; Shewmaker et al., 2006), suggest that the

Sup1–40 core may resemble the Sup35 peptide structures, with the exception that the dry sheet–sheet interfaces are probably formed by intramolecular interactions between beta-sheet faces from different rather than identical Asn/Gln-rich regions. Because some differences in protection patterns within Sup1–40 are observed between Sc4 and Sc37, these two strains may have distinct sheet–sheet interfaces in which the Sc37 arrangement accommodates additional beta-sheets from the oligopeptide repeats. Such diverse sheet–sheet interfaces have recently been described in peptide structures (Sawaya et al., 2007).

Our finding that the Gln/Asn-rich Sup1–40 subdomain forms an overlapping amyloid core that expands well into the adjacent oligopeptide repeats in a strain-dependent manner provides a structural rationale for several diverse functional studies. First, mutational studies and a recent peptide-mapping analysis indicate that prion formation and specificity of growth are particularly sensitive to changes within Sup1–40 (refs 24–26). Second, the SupNM prion domain has a modular architecture in which Sup1–40 is specifically required for amyloid formation and templated growth, and can be functionally replaced by amyloidogenic stretches of pure polyGln repeats (Osherovich et al., 2004). In addition to a role for a subset of the oligopeptide repeats in stabilizing amyloid structure, these repeats seem to have a distinct and essential function in allowing chaperone-mediated replication of such amyloids, thereby generating new prion seeds. This role in prion division can be replaced by a number of diverse sequences (Crist et al., 2003; Parham et al., 2001). The less stable structure over much of the oligopeptide repeats in addition to their more diverse sequence composition may facilitate recognition of this region by chaperones (Tuite and Cox, 2006). Last, the structural differences

observed here shed light on how conformations alter in vivo phenotypes as well as leading to strain-specific sequence requirements for prion propagation. Ordering of the first three oligopeptide repeats in Sc37 is associated with increased stability of these fibres (Tanaka et al., 2004; Tanaka et al., 2006) and may also occlude chaperone recognition sites. Taken together, these findings account for the observation that the weaker strain phenotype of Sc37 prions results from a difficulty in generating new prion seeds despite robust fibre growth. Previous studies also found that an increased number of oligopeptide repeats (four versus two) was minimally required to support the propagation of a 'weak' strain as compared with a 'strong' strain (Shkundina et al., 2006). Thus, for both strains, [*PSI*$^{+}$] propagation seems to require at least one oligopeptide repeat outside the highly protected core. The mammalian prion protein, PrP, contains peptide repeat regions reminiscent of Sup35, whose number modulates prion propensity even though they lie outside the protease-resistant prion core (Cohen and Prusiner, 1998). This raises the possibility that these otherwise unrelated prion proteins share a common functional architecture in which an amyloid core mediates templated growth, and less stably structured regions facilitate the generation of new prion seeds.

Note added in proof: Mutation analysis indicated that of the 23 glycines, only the 2 present in the M domain were visible by solution NMR of uniformly labelled fibres, which is consistent with the conclusion that the M domain is highly mobile.

Methods Summary

SupNM isotope labelling

Labelled SupNM was expressed in Escherichia coli.

NMR on fibres

SupNM fibres uniformly labelled with ^{15}N, or specifically labelled with ^{15}N-Leu, were seeded and polymerized at 4 °C as described (Tanaka et al., 2004). Fibres were spun down and resuspended in 1/40 volume of equivalent buffer in 10% (v/v) D_2O (pH 5.5 for uniformly labelled). Standard ^{15}N-HSQC spectra were recorded at 800 MHz. The final protein concentration is estimated as 200 μM. Only a few peaks with chemical shifts typical of glycine were seen in the uniformly labelled sample. The failure to detect all 23 glycine residues in SupNM indicates that the peaks observed were from fibres rather than from a monomer subpopulation.

H/D exchange

H/D exchange was performed on ^{15}N-SupNM seeded fibres largely as described (Hoshino et al., 2002), with time points at 0 min, 1 min, 1 h, 1 day and 1 week of exchange. For NMR measurements, fibre pellets were dissolved in dissolution buffer (95% DMSO-d_6, 4.5% D_2O, 0.5% dichloroacetic acid-d_2 (v/v) and 200 μM 2,2-dimethyl-2-silapentane-5-sulphonate sodium salt (DSS) at pH 5.0) and ^{15}N-HSQC correlation spectra were recorded at 800 MHz and 298 K. Dichloroacetic acid-d_2 was purchased from CDN Isotopes. Spectra were recorded in accordance with the strategy described (Yamaguchi et al., 2004). Additionally, a one-dimensional ^{1}H spectrum was acquired after ^{15}N-HSQC.

Mutagenesis studies

All mutant plasmids were generated, overexpressed and purified as described (DePace et al., 1998; Tanaka et al., 2004). ThioT assays were performed as described(Chien et al., 2003). Sc4 and Sc37 seeded reactions were performed at 4 °C and 25 °C, respectively. Initial rates were calculated from the first 16 min of polymerization. AFM assays were performed as described (DePace and Weissman, 2002).

Full methods accompany this paper.

Acknowledgements

We thank M. Tanaka, C. Ritter, M. Hoshino, W. Bermel and R. Riek for experimental advice; and D. Breslow, D. Cameron, S. Collins, V. Denic, K. Filaski, C. Foo, C. Gross, J. Hollien, N. Ingolia, E. Quan, E. Rodriguez and K. Tipton and other members of the Weissman laboratory for helpful discussion and critical reading of the manuscript. This research was funded by the NIH and the Howard Hughes Medical Institute.

Backbone assignments of SupNM have been deposited in the Biological Magnetic Resonance Data Bank, accession number 15379.

Competing interests statement

The authors declare no competing financial interests.

Online Methods

SupNM isotope labelling

Uniformly ^{15}N labelled SupNM was overexpressed by growing 3 l of the bacterial strain BL21/DE3 harbouring a plasmid encoding SupNM-His6x under control of the T7 promoter, to a D600 value of 0.3 in Luria–Bertani medium at 37 °C as described (Santoso et al., 2000). Cells were spun down, washed once in 10 ml of ^{15}N-M9 medium, and resuspended in 1 l of ^{15}N-M9 medium. After 30 min at 37 °C, expression was induced by the addition of 400 μM isopropyl beta-d-thiogalactoside and after 4 h the cells were harvested. Uniformly labelled ^{13}C,^{15}N-SupNM was overexpressed in the same manner, using 1 g of ^{13}C-glucose per litre of M9 medium. ^{15}N-Lys-SupNM protein was overexpressed as described above with medium supplemented with ^{15}N-Lys. Specifically labelled ^{15}N-Glx-, Asn/Asp (Asx)-, Tyr-, Phe-, Leu- and ^{13}C,^{15}N-Glx,Asx/Tyr-SupNM proteins were overexpressed as described above by using the bacterial strain DL39 with M9 medium supplemented with the indicated ^{15}N amino acid (Asp and Glu for Asx and Glx, respectively) as well as all other amino acids unlabelled as described (Muchmore et al., 1989). All ^{15}N-labelled and ^{13}C-labelled amino acids were purchased from Isotec. Protein purification was performed as described (DePace et al., 1998).

H/D exchange

^{15}N-SupNM seeded fibres of each strain were made as described (Tanaka et al., 2004) and spun down at 150,000g for 1 h and resuspended in the equivalent buffer in D_2O at pH 2.5. Fibres were then passed through a 22-gauge needle to generate short fibres of relatively uniform size (about 100–300 nm) as assayed by AFM. To start the exchange, the pH was adjusted to 7.0. After the desired time, the pH was adjusted back to 2.5 and fibres were centrifuged at 126,000g for 25 min. The pellet was washed once with 5 mM

DCl in D_2O and then centrifuged again at 126,000g for 20 min. The pellet was then frozen, freeze-dried, and stored at -80 °C until NMR acquisition. All steps, including H/D exchange, were performed at 4 °C. Fibre conformation purity was assayed by infecting samples from before and after the H/D exchange time course into [*psi*$^-$] and the conformation was determined by 'weak' or 'strong' colour phenotype as described(Tanaka et al., 2004). All preparations were of greater than 95% purity as judged by this method. The NMR spectra were processed with nmrPipe (Delaglio et al., 1995), and peak integrations were performed with Sparky (Goddard and Kneller). Each ^{15}N-HSQC spectrum for the time course was normalized for protein concentration by using integrations of the unexchangeable side-chain peaks in comparison with the internal DSS standard in the one-dimensional control spectra. Exchange of fibres occurred mainly at neutral pH, because when the pH was left at 2.5, peak intensities decreased slightly, which is consistent with predicted intrinsic rates at 4 °C and pH 2.5, and exchanged to a much fuller extent after the pH had been shifted to 7.0 (data not shown). Estimated minimum peak intensity was calculated by averaging the baseline for the fitted curves of the fastest-exchanging residues. Sequence-specific assignments of the backbone Hn and N resonances were achieved with triple-resonance three-dimensional HNCO, HN(CA)CO, CBCA(CO)NH, HNCACB, HN(CA)NH and CT-HNCA (Sattler et al., 1999), on uniformly labelled ^{13}C,^{15}N-SupNM. HNCO, CT-HNCA, HN(CA)NH and HN(COCA)NH experiments were also performed on SupNM specifically labelled with ^{13}C,^{15}N-Glx and ^{13}C,^{15}N-Asx/Tyr. HNCO, CT-HNCA and HN(COCA)NH experiments used semi-constant time ^{15}N evolution to increase resolution (Sun et al., 2005). Three-dimensional ^{15}N-separated HSQC-nuclear Overhauser enhancement spectroscopy (tm =

400 ms) and HSQC-total correlation spectroscopy (tm = 100 ms) experiments were also performed on uniformly labelled ^{15}N-SupNM and on specifically labelled ^{15}N-Asx, Lys, Glx and Tyr-SupNM. All spectra were recorded on Bruker Avance800 or DRX500M spectrometers equipped with cryoprobes with actively shielded Z gradients at 298 K. Assignments were performed with the program ansig (Kraulis, 1989).

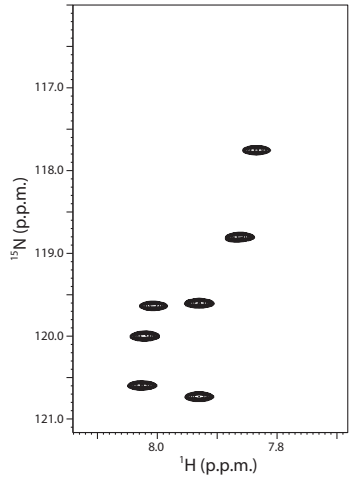

Figure 3.4 ^{15}N-HSQC spectrum of ^{15}N-leucine specifically labelled SupNM monomers in DMSO dissolution buffer.

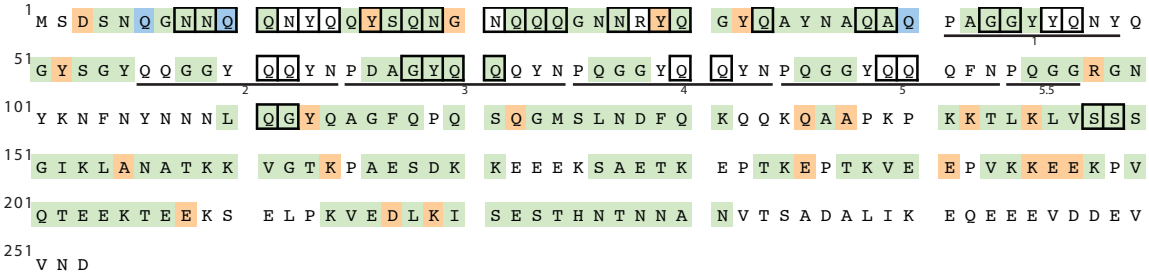

Figure 3.5 Sequence assignment of SupNM.
Plotted is the SupNM sequence along with assignments. In green are residues that are assigned and are non-overlapping or unambiguous. In orange are residues that are assigned, but exhibit overlap with other peaks rendering them ambiguous. In blue are peaks that are assigned and are non-overlapping in ^{15}N-Glx specifically labelled protein. Underlined residues indicate the oligopeptide repeats with their corresponding number. Boxed residues are those that were mutated to prolines for the mutagenesis study.

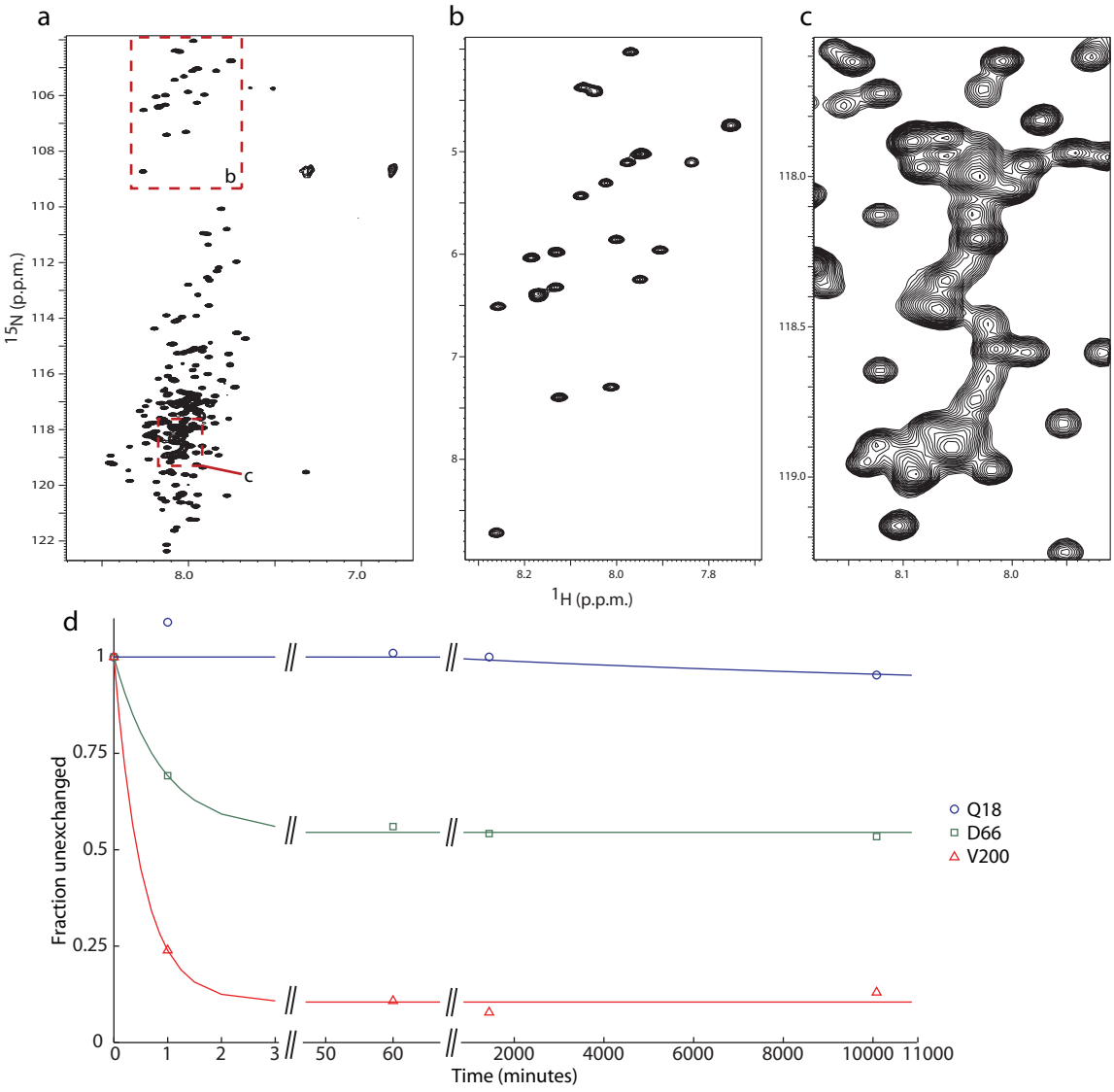

Figure 3.6 H/D exchange spectra and curves.

a, ^{15}N-HSQC of uniformly ^{15}N labelled SupNM acquired in 95% DMSO-d_6, 4.5% D_2O, and 0.5% dichloroacetic acid-d_2. b, Zoomed in view of the glycine residues, indicated by the box in panel a. c, Zoomed in view of a region with significant spectral overlap, location indicated in panel a. d, Representative H/D exchange data (symbols) for three classes of residues with their corresponding fit curves (lines). In blue circles are residues that experience little or no exchange over the entire timecourse such as Q18. In green squares are residues such as D66 that experience fast initial exchange, but remain stable at an intermediate exchanged level for the remainder of the time course. In red triangles are residues such as V200 which exchange very quickly by the first time point and remain unchanged for the course of the experiment. Curves are from H/D exchange data on the Sc37 conformation.

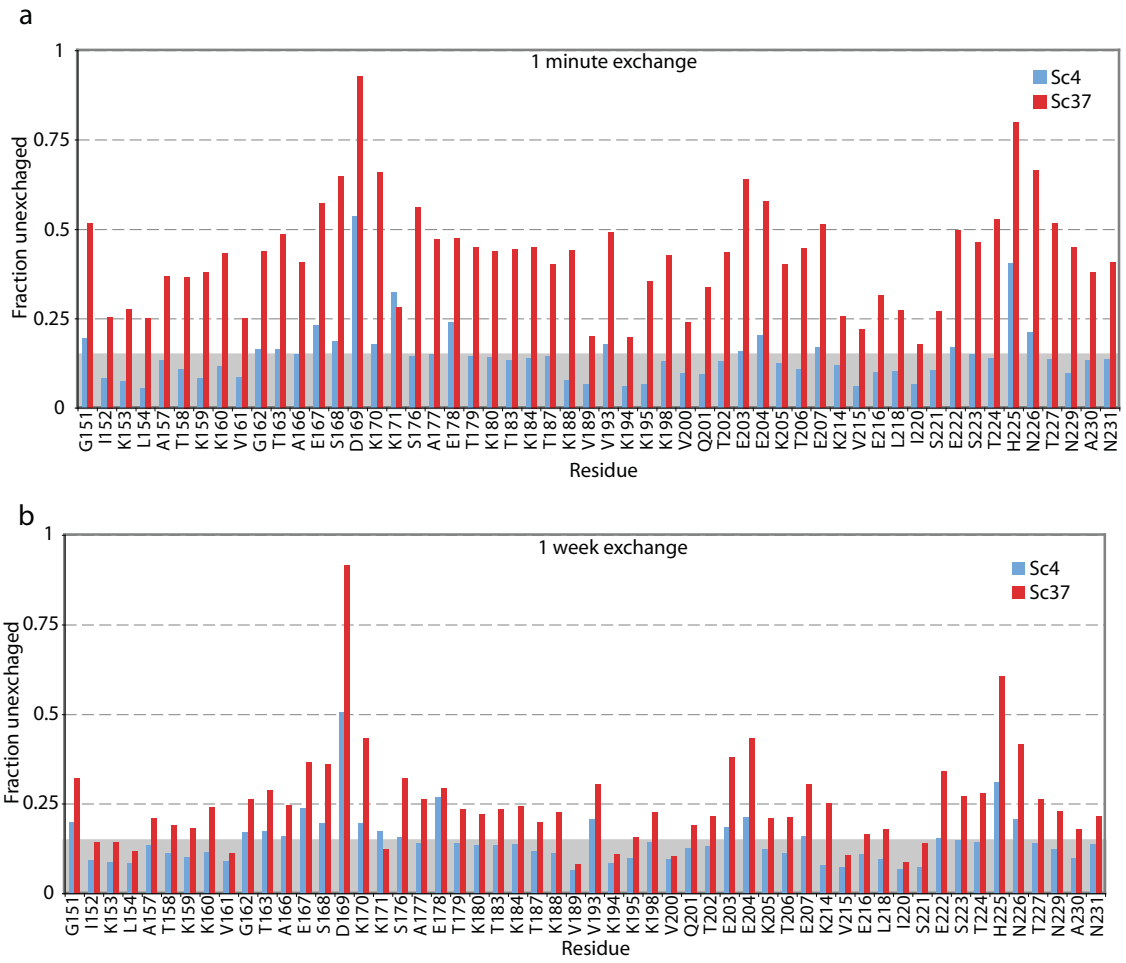

Figure 3.7 H/D exchange for residues 151-231.
Fractions unexchanged are displayed for residues 151-231 after one minute (a) and one week (b) of exchange as described in the text.

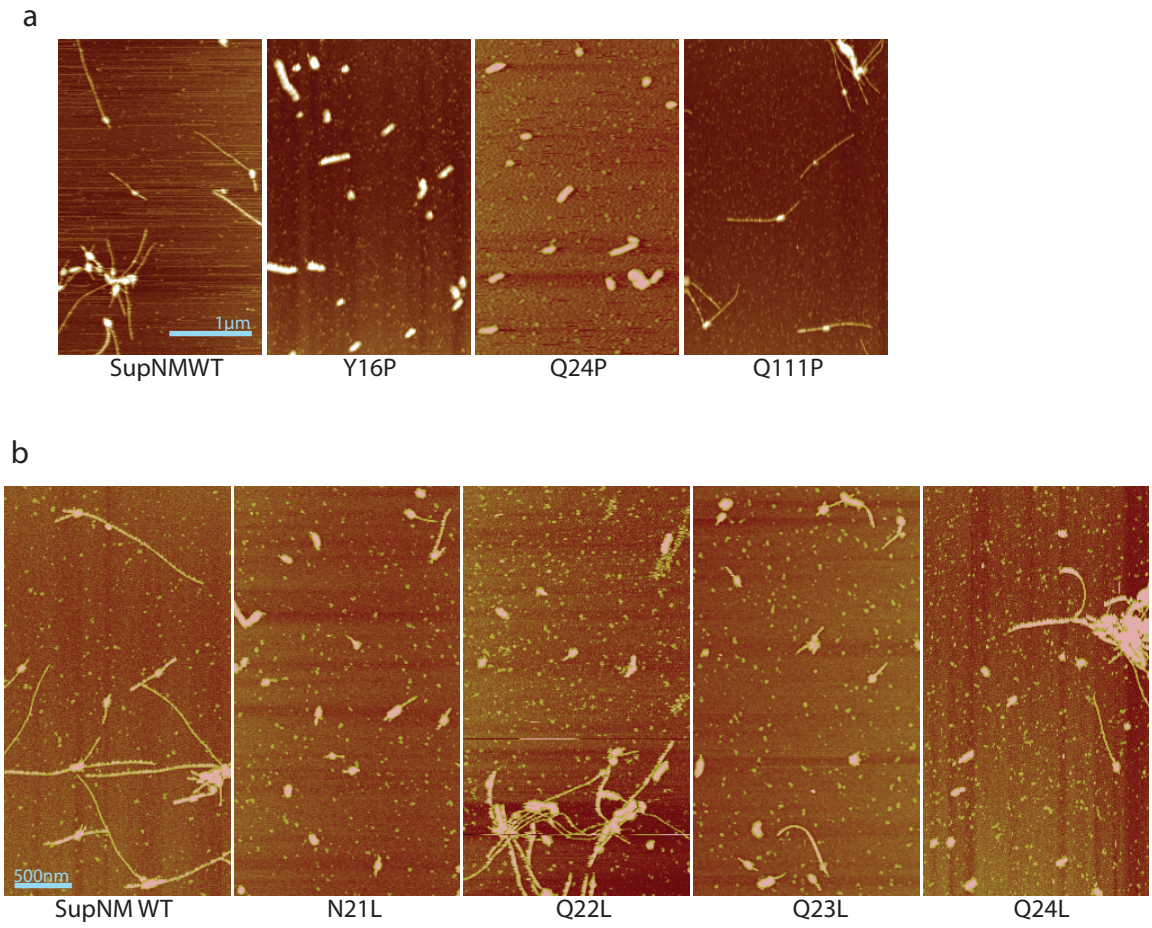

Figure 3.8 AFM of mutant polymerization.
Wildtype Sc4 seed tagged with HA was added to the indicated untagged proline (a) and leucine (b) mutant proteins and allowed to polymerize for 10 minutes. Reactions were then deposited onto mica, and HA antibody added to distinguish the seed (wide areas of the fibres) from the fibre growth (narrow area of the fibres). Samples were then imaged by AFM.

Chapter 4

Unpublished data

Chaperone recognition elements on SupNM

Brandon H. Toyama[1] and Jonathan S. Weissman[1]

[1]Howard Hughes Medical Institute, Department of Cellular and Molecular Pharmacology, University of California-San Francisco and California Institute for Quantitative Biomedical Research, San Francisco, California 94158-2542, USA.

Introduction

Prions, like any other cellular aggregate, do not act alone. Rather, they are just as prone to the cellular quality control machinery, namely the molecular chaperones, as any other protein resident in the cell. The yeast prions have the unique property of actually being dependant on chaperones, where deletion of one in particular, Hsp104, results in loss of the prion phenotype (Alberti et al., 2009; Chernoff et al., 1995; Moriyama et al., 2000; Sondheimer and Lindquist, 2000). Subsequent studies showed that in addition to Hsp104, the chaperones Ssa1 and Sis1 also play a role upstream to Hsp104 in the maintenance of the [*PSI*$^{+}$] prion (Bagriantsev et al., 2008; Jones and Tuite, 2005; Tipton et al., 2008). Although the exact binding sites of these chaperones on SupNM fibers is not known, it has been hypothesized that they recognize the oligopeptide repeat region (Osherovich et al., 2004). This was due to the observation that the oligopeptide repeats were necessary for the propagation of the prion, but could not aggregate on their own. The previously described structural studies added support to this hypothesis, in that the oligopeptide repeats were found to be largely unstructured and thus more accessible to chaperone recognition and binding. Furthermore, a different number of oligopeptide repeats were found to be structured between the two studied Sc4 and Sc37 strains, opening the possibility of differential chaperone recognition playing a role in prion strain phenotypes. These unpublished data aimed to establish an *in vitro* system in which to map out potential binding sites of the Ssa1 and Sis1 chaperones on SupNM fibers.

Results and Discussion

Ssa1 and Sis1 binding

The Ssa1-6xHis chaperone was purified to homogeneity from a *pichia pastori* strain generously provided from Johannes Buchner's laboratory through Ni^{2+}-NTA agarose affinity chromatography followed by ion exchange chromatography on a ResourceQ column. Sis1 chaperone was cloned into a N-terminal 6xHis construct and purified to homogeneity using Ni^{2+}-NTA agarose affinity chromatography, gel filtration chromatography using a SD200 column, and ion exchange chromatography using a ResourceQ column. Ssa1 displayed ATPase activity (data not shown) and was tested for its ability to bind SupNM Sc4 fibers with Sis1 *in vitro* using dynal beads conjugated with anti-SupNM antibody. In this assay, Sc4, Ssa1, and Sis1 were incubated in the presence of no nucleotide, ADP, ATP, and AMPPNP at 30°C for 10 minutes. Dynal beads were then added and the reaction incubated on ice for 30 minutes with occasional mixing. Beads were washed 3 times and eluted by adding SDS sample buffer and boiled. The elution was run on and SDS-PAGE and stained. Sis1 bound resin in a non-specific manner. However, Ssa1 bound Sc4 fiber only in the presence of ATP in a Sis1 dependant manner (Fig. 4.1). This demonstrated the ability to decorate SupNM fibers with the Ssa1 chaperone. Whether Sis1 bound SupNM fibers could not be determined from this assay. With this ability, a number of strategies were employed to try to identify the chaperone recognition elements on SupNM.

Mapping chaperone binding by H/D exchange

The first method used was the H/D exchange assay developed in the previous chapter (Toyama et al., 2007). The rationale for this was that chaperone binding may result in a small amount of protection from exchange of residues that the chaperone is

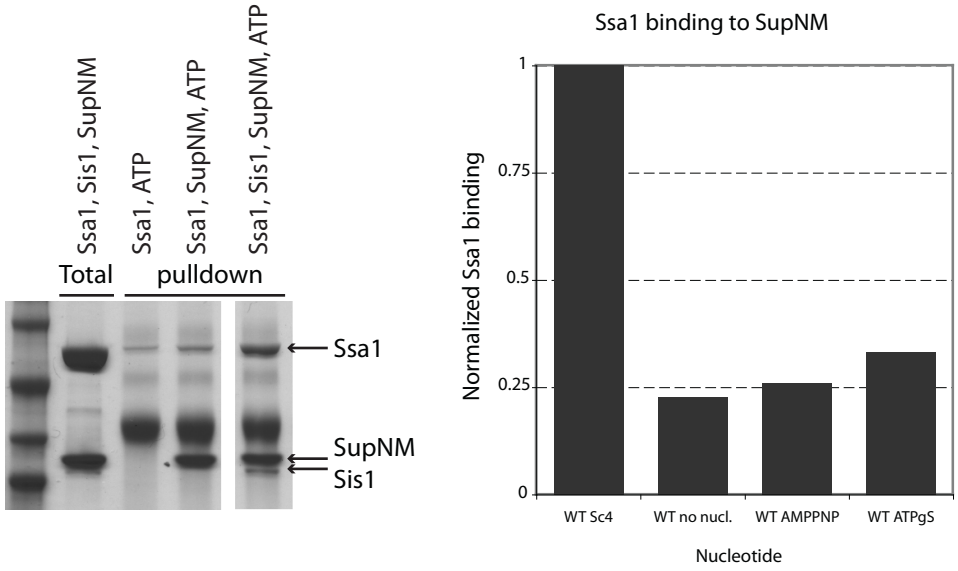

Figure 4.1 Ssa1 interation with SupNM fibers

Left: Ssa1 was incubated with beads alone, with SupNM fibers, or with Sis1 and SupNM fibers. Bound SupNM fibers were pulled down, and the complex run on a gel.

Right: Quantitation of a pulldown performed as described above. Amount of bound Ssa1 was normalized to the amount bound to WT Sc4 in the presence of ATP.

interacting with. Thus, the H/D exchange protocol was adjusted to accommodate exchange with chaperones. Briefly, ^{15}N-SupNM fibers were incubated with molar equivalents of Ssa1 and Sis1 and nucleotide, and this solution was concentrated to 1/10th the exchange volume. To start exchange, D_2O buffer was added to dilute the concentrated sample 10-fold, and the assay was performed from this point on as previously described. H/D exchange results did not provide any insights into chaperone binding sites on SupNM fibers. Exchange was performed twice. For the first attempt, the chaperone binding data did not differ from the negative controls (data not shown). For the second attempt, marginal protection was observed in the chaperone sample over the negative control, however, this difference is small and may not be significant (Fig. 4.2). Observation of protection due to chaperone binding might not be present for a number of reasons. First, the chaperones, particularly Sis1, are prone to misfolding and aggregation upon large buffer changes and sudden dilution. Thus, when the concentrated fiber/chaperone mixture was diluted with D_2O buffer, the solution became extremely cloudy, suggesting a significant population of unfolded and aggregated protein. Thus, any chaperone interactions may have been lost at this step. Furthermore, based on crystal structures of the bacterial homologue DnaK in complex with a substrate peptide, at most two backbone amide protons on the peptide were engaged in a hydrogen bond to the chaperone (Zhu et al., 1996). Thus, if Ssa1 binds SupNM fibers at a specific spot, you would only expect two residues to display protection in the presence of chaperones. Also, not all residues in SupNM have been assigned or are non-overlapping, chaperones most likely bind SupNM sub-stoichiometrically (Bagriantsev et al., 2008), and binding conceivably could be spread across multiple recognition sites. All these factors make the

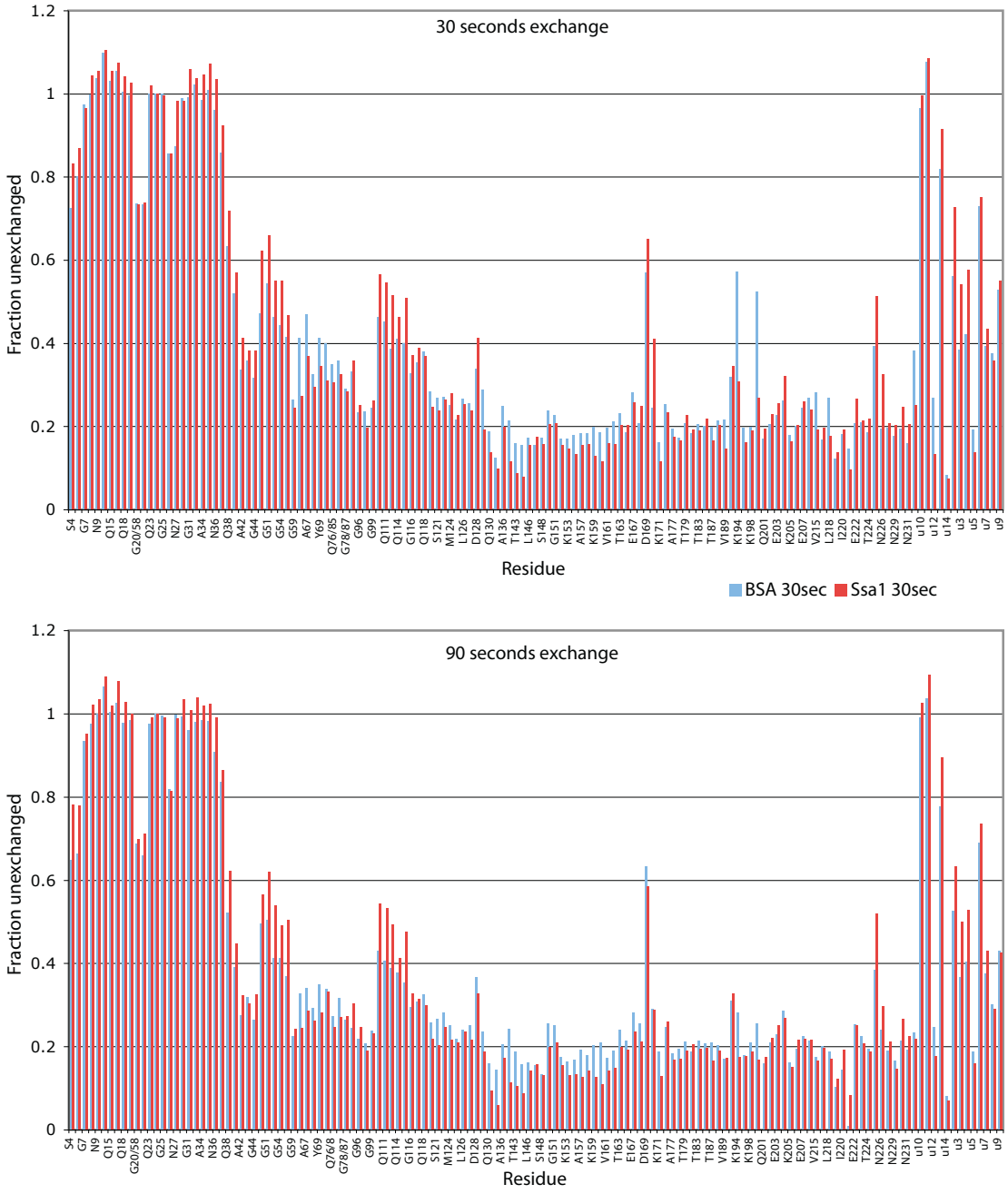

Figure 4.2 Chaperone binding mapped by H/D exchange

Intensities for all unambiguous peaks as a fraction of the non-exchanged intensity after 30 seconds (upper) and 90 seconds (lower) of exchange for Sc4/BSA (blue) and Sc4/Ssa1/Sis1 (red) reactions as described in the text.

prospects of identifying the chaperone binding site through protection from H/D exchange not likely.

Mapping chaperone binding by mutagenesis

Another strategy used to map chaperone binding to SupNM fibers is by using point mutants in SupNM. The previous study resulted in a library of over 100 point mutants in SupNM (Toyama et al., 2007). Since we have an *in vitro* binding assay to monitor Ssa1 interactions with SupNM fibers, we reasoned that a mutation that lays within the chaperone recognition site may disrupt chaperone/fiber interactions, which may be observed through the binding assay. We therefore performed the binding assay with a number of different SupNM mutants across regions predicted to be unstructured by H/D exchange. Studies on the binding preference of DnaK found that large negatively charged residues such as glutamate and aspartate as well as proline were disfavored for binding (Rudiger et al., 1997). Thus, we first attempted to monitor binding of Ssa1 to proline mutants located in the oligopeptide repeats, the predicted binding sites (Fig. 4.3a). Although reduced binding to various mutant SupNMs could be observed, the results varied from day to day, and a mutant that would be predicted to not interfere with Ssa1 binding based on its location, S149P, also displayed reduced binding occasionally. Due to the inconsistency, these data were thus taken as not significant. The acidic residues are even more disfavored for binding Ssa1, thus, we tried the same binding assay with residues mutated to glutamate (Fig. 4.3b). This however, yielded similar results to the proline mutants in that the results were not consistent. Finally, we hypothesized that perhaps mutating one residue might not have a large effect since the other oligopeptide

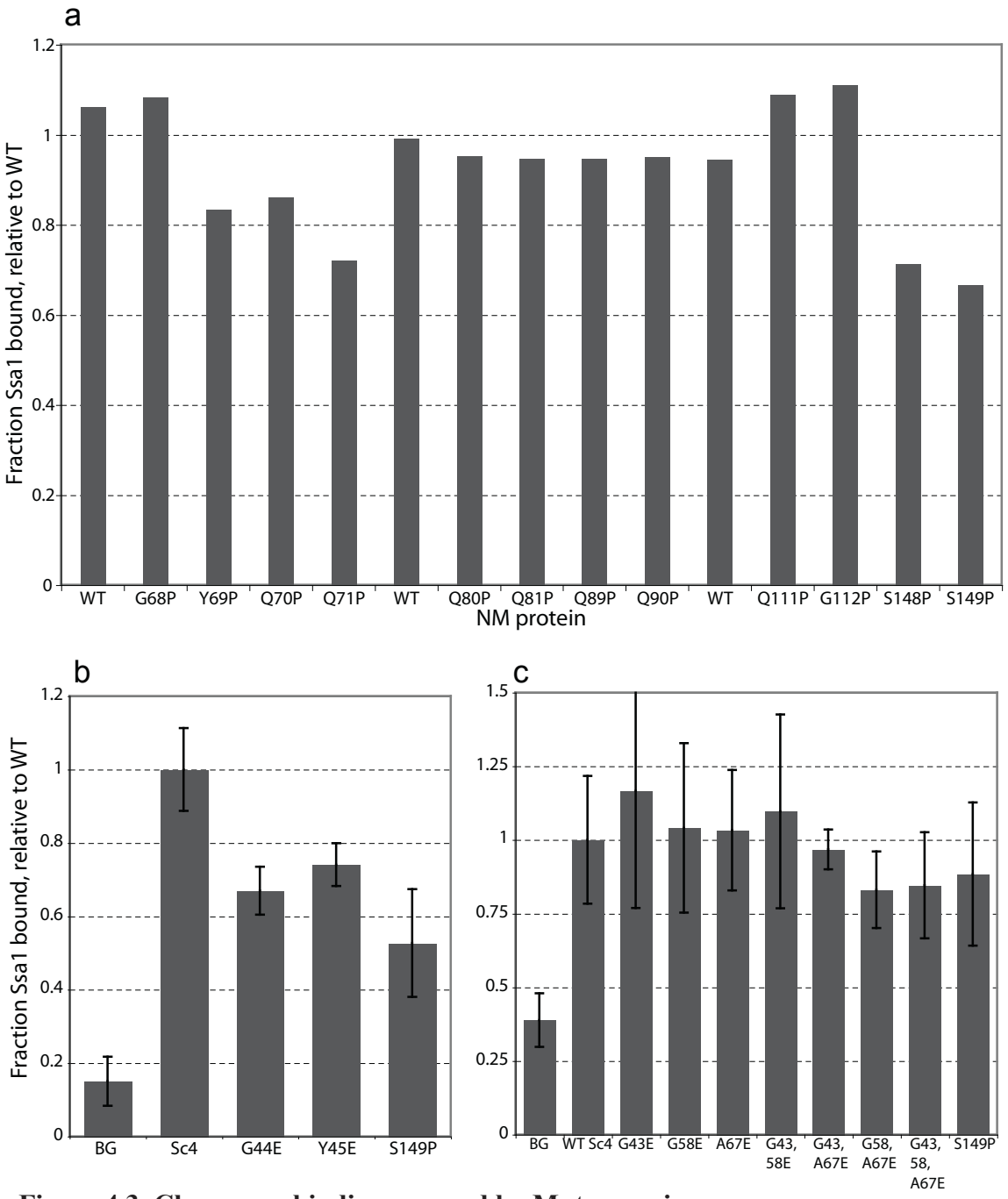

Figure 4.3 Chaperone binding mapped by Mutagenesis

a, Indicated SupNM proline mutants were tested for their ability to pull down Ssa1, as described earlier. Plotted are quantities of Ssa1 pulled down with each mutant, normalized to WT SupNM. b, The above pulldown was performed with the indicated glutamate mutants of SupNM. Error bars represent the standard deviation from three replicates. c, The above pulldown was performed on the indicated single, double, and triple glutamate mutants. Error bars represent the standard deviation from three replicates.

repeats could compensate as binding sites. Thus, we tried binding assays with double and triple mutants where multiple residues in the same position of different oligopeptide repeats were mutated (Fig. 4.3c). The prediction would be that as you mutated more residues, you would see less binding. This, however, was not seen as all mutants displayed similar levels of binding Ssa1 under these conditions. In all, the *in vitro* binding did not appear to be a robust enough assay to accurately reflect different affinities of binding to SupNM mutants. Thus, another method was sought.

Mapping chaperone binding by acrylodan fluorescence

An alternative way to map binding is through changes in fluorescence properties. The fluorophore acrylodan changes its emission maxima and intensity in response to changes in its local environment. This property was used as a proxy to observe DnaK binding to an acrylodan labeled peptide (Pierpaoli et al., 1998; Schmid et al., 1994). Upon DnaK binding, the authors observed a corresponding shift in maximal fluorescence and a dramatic increase in fluorescence intensity. We speculated that this potentially could be used to map binding sites of Ssa1 on SupNM fibers. Previous studies have yielded a large library of cysteine point mutations scattered throughout the SupNM sequence (Tanaka et al., 2004; Tanaka et al., 2005). By labeling each of these mutants with acrylodan on the cysteine side-chain, binding in the vicinity of the label should result in an increase in fluorescence intensity. Thus, which cysteine mutants result in the fluorescence increase would tell us where the chaperone is binding. A number of SupNM cysteine mutants were therefore labeled with acrylodan, and their fluorescence emission spectra determined individually with and without Ssa1/Sis1 (Fig. 4.4). Only

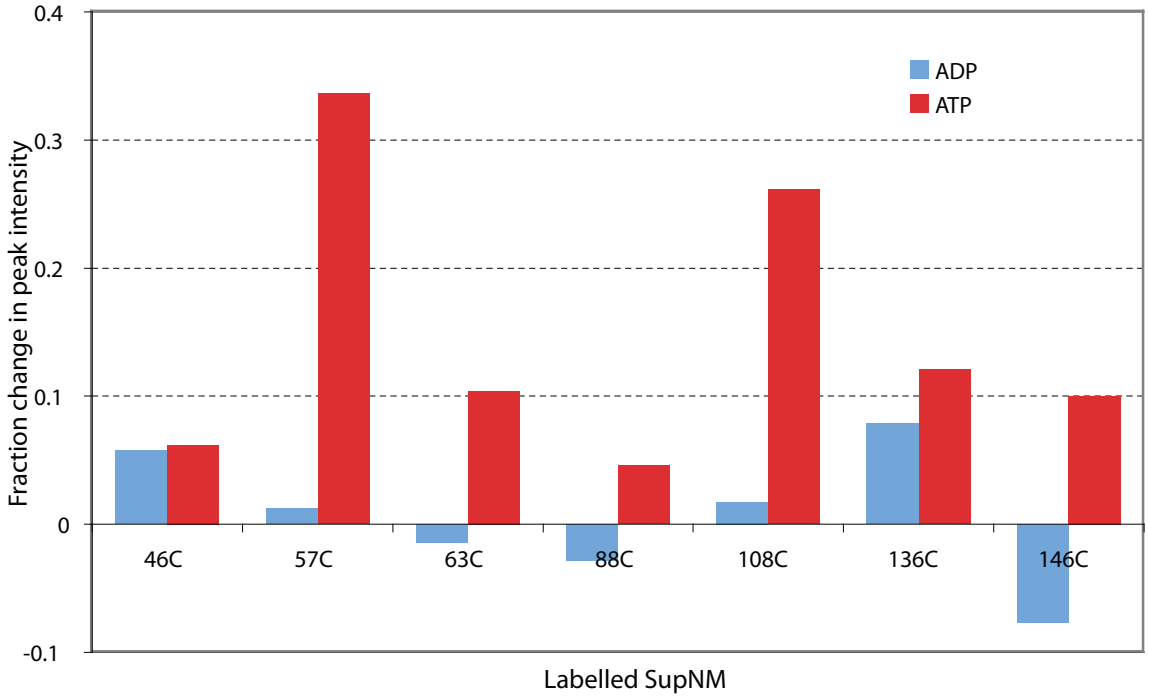

Figure 4.4 Chaperone binding mapped by acrylodan fluorescence

Indicated SupNM cysteine mutants were tested labeled with acrylodan, and fluorescence emission spectra aquired in the presence of ADP or ATP, with or without Ssa1 and Sis1. The difference in peak fluorescence emission was determined, and is plotted as a fraction of total peak emission for the ADP and ATP conditions.

one mutant seemed to show significant fluorescence intensity increase. This mutation happens to be very close to the SupNM mutant PNM2 (G58D), which is known to aggregate properly, but potentially have perturbed chaperone interactions (Osherovich et al., 2004). Thus, these data seemed plausible that chaperones were binding at this oligopeptide repeat.

Conclusions

An *in vitro* system for observing Ssa1/Sis1 chaperone binding to SupNM fibers was successfully established. A number of attempts to map the chaperone binding sites on SupNM fiber, however was not successful due to sensitivity limitations. Mapping by acrylodan fluorescence was successful, but at limited resolution. Further refining the binding site will require a number of other point mutants to confirm Ssa1/Sis1 binding in this vicinity.

Oligomers of SupNM

Motomasa Tanaka[2,3], Brandon H. Toyama[1], and Jonathan S. Weissman[1]

[1]*Howard Hughes Medical Institute, Department of Cellular and Molecular Pharmacology, University of California-San Francisco and California Institute for Quantitative Biomedical Research, San Francisco, California 94158-2542, USA.*

[2]*PRESTO, Japan Science and Technology Agency, 4-1-8 Honcho Kawaguchi, Saitama 332-0012, Japan*

[3]*RIKEN Brain Science Institute, Hirosawa2-1, Wako, Saitama351-0198, Japan*

Introduction

Ever since the observation that a different conformation of prion fiber (Sc4) would form if spontaneous polymerization was initiated at 4°C, the first question most people have is, "Why?" This is the question Motomasa Tanaka and co-workers have been trying to address. His preliminary studies have found that at 4°C, SupNM monomer reversibly forms an oligomeric structure that is not congruent to the Sc4 fiber structure (Ohhashi et. al., 2009, submitted). If the temperature of the oligomer is raised to close to 25°C, it immediately dissociates into single monomers. Tanaka and co-workers have also found that the oligomer is on-pathway to fiber formation. In an effort to better characterize the oligomeric structure, Tanaka and co-workers have collaborated with us to study this process by NMR. These unpublished data are experiments performed in collaboration with Motomasa Tanaka in an effort to better understand SupNM oligomer structure.

Results and Discussion

In collaboration with Motomasa Tanaka, we sought to try to determine secondary structure of the SupNM oligomer by H/D exchange. The protocol was again modified to accommodate this. Briefly, an appropriate amount of ^{15}N-SupNM monomer was put over a reverse-phase HPLC column to remove the guanidine it is stored in. The sample was then frozen and lyophilized. The dried monomer was resuspended in pure D_2O at 4°C and allowed to exchange for a short period of time. Exchange was quenched by freezing the sample in liquid nitrogen, and was then lyophilized. The data acquisition and processing was then performed as described. As shown in figure 4.5, no appreciable

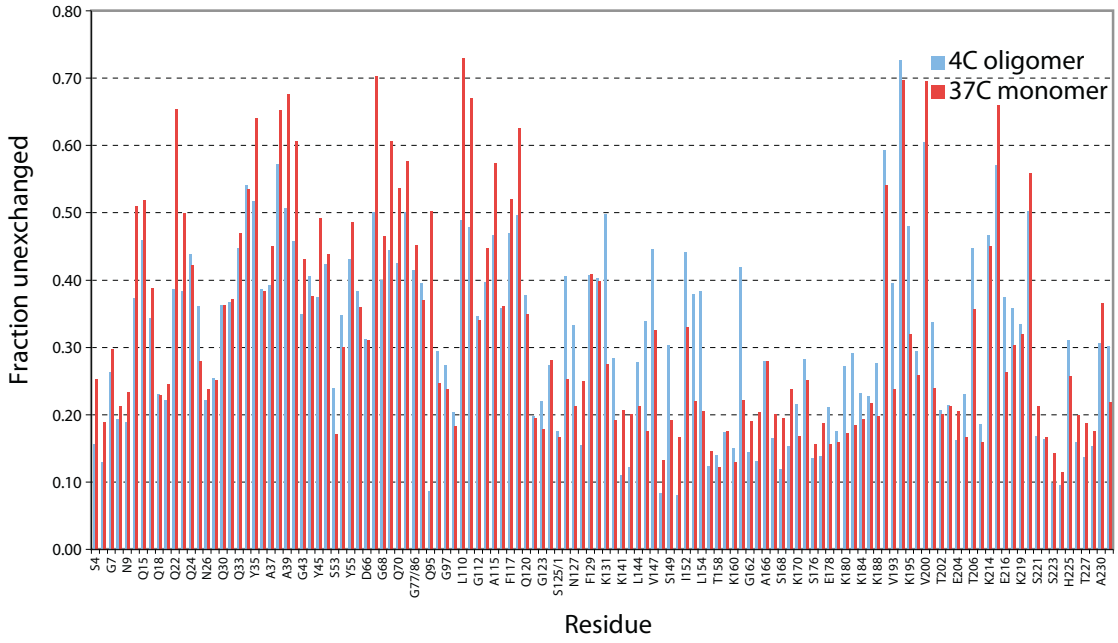

Figure 4.5 Oligomer structure by H/D exchange

Intensities for all unambiguous peaks as a fraction of the non-exchanged intensity are plotted for SupNM at 4ºC (oligomer) and 37ºC (monomer). Exchange for monomer was performed for 1 minute as opposed to 22 minutes for the oligomer to compensate for the different rates of intrinsic exchange at the respective temperatures.

protection was observed for the oligomeric structure. There are a number of reasons this might occur. First, as we had no way to confirm the presence of oligomer during exchange, the oligomer may not have formed for whatever reason. Second, the structure may be very weak, and thus not result in significant protection. Finally, the oligomeric structure is very dynamic in nature (Tanaka, unpublished observations) and thus any protection may have been quickly lost as oligomers quickly dissociated and re-associated.

Alternatively, we thought we might be able to observe oligomer formation by NMR. The previous study was able to do limited experiments using solution NMR on SupNM fibers (Toyama et al., 2007). The only peaks visible corresponded to residues that were unstructured. Similarly, we thought we might see peaks disappear as oligomer formation occurs, the only remaining peaks again corresponding to residues unstructured in the oligomer structure. This indeed was the case, as a ^{15}N-SupNM sample at 25°C appeared as a monomer, resulting in a nicely dispersed spectrum (Fig. 4.6). When the same sample was lowered to 8°C, a number of peaks disappeared which is exactly what we would have expected upon oligomer formation. This process was reversible, as all the peaks reappeared upon raising the same sample back to 25°C. Quantitation of randomly picked peaks shows that the vast majority of peaks are lower in volume upon oligomer formation, with many completely disappearing from the spectrum. When the sample was returned to 25°C, however, the peak volumes all returned remarkably close to the original peak volume.

Another way to confirm oligomer formation by NMR is through a NOESY. In this experiment, crosspeaks represent through-space interactions between nuclei that are in close proximity. Thus, as the oligomer forms, the monomers should become more

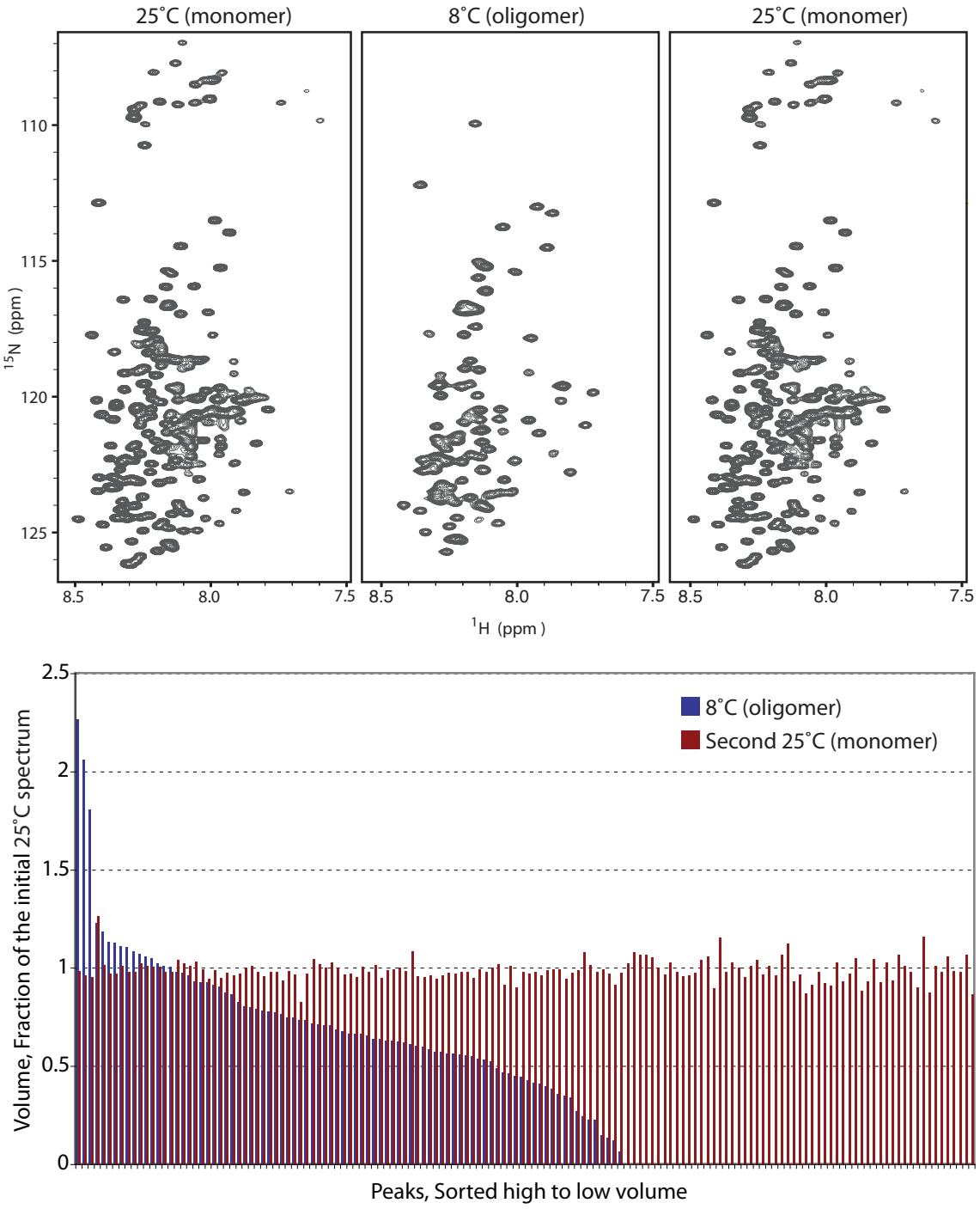

Figure 4.6 Oligomer formation observed by solution NMR

Upper: Lyophilized SupNM monomer was dissolved in buffer and an HSQC spectrum aquired at 25ºC. The sample was then shifted to 8ºC and another spectrum aquired. The sample was then raised bact to 25ºC and a final spectrum aquired. Lower: Quantitation of peak volumes normalized to the initial 25ºC spectrum peak volumes, sorted from higher fractions to lower fractions.

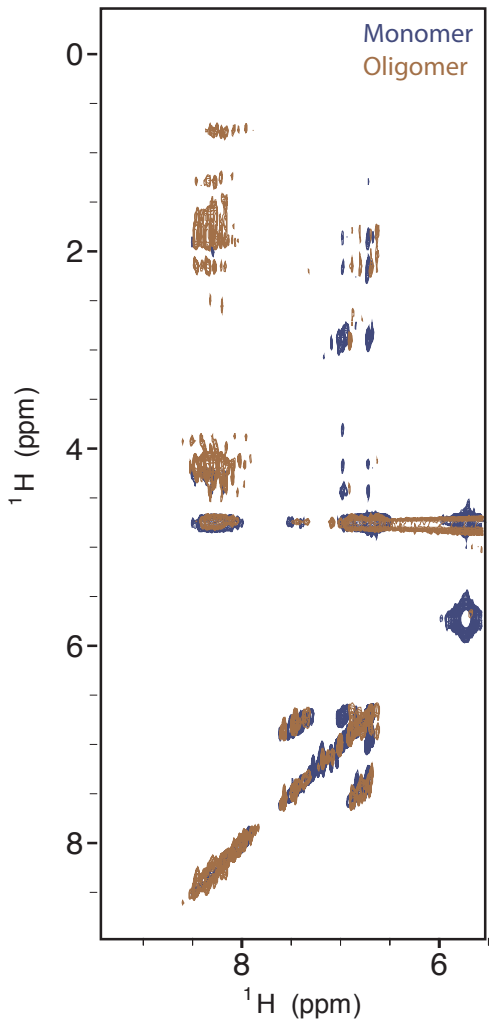

Figure 4.7 Oligomer formation by NOESY

Lyophilized SupNM monomer was dissolved in buffer and a NOESY spectrum aquired at 25ºC (dark blue). The sample was then shifted to 17ºC and another spectrum aquired (red). Plotted is the regions highlighting NOEs between the amide protons and sidechain protons.

structured resulting in more potential NOEs. This would be observed as an increase in crosspeak signal on a NOESY spectrum. NOESY spectra were therefore acquired on a SupNM sample at 25°C and 8°C (Fig. 4.7). The spectra at 8°C clearly shows a large increase in NOEs over the 25°C spectrum, again demonstrating the formation of higher order structure at the lower temperature.

Conclusions

This demonstrated that not only could you observe oligomer formation by solution NMR, but that it was fully reversible. Furthermore, you could observe on residue-level resolution, which peaks may be participating in the oligomer fold, and also potentially specific through-space contacts. What remains, is assignments of the monomeric spectrum. This would allow you to know exactly which residues in SupNM participate in the oligomer, and which do not.

Chapter 5

Summary

Summary

In summary, we have been able to first demonstrate that two yeast prion strains, Sc4 and Sc37, represent two conformations of fiber that have distinct physical properties (Tanaka et al., 2004; Tanaka et al., 2006). Sc4 fibers polymerize slowly at physiological temperatures and form fragile fibers. Sc37, however, robustly polymerize at physiological temperatures and form strong fibers that are more resistant to breakage (Tanaka et al., 2006). Subsequent structural studies then identified the residue-specific conformational differences between these fibers, revealing an overlapping amyloid core but expansion of structure in the Sc37 conformation that almost doubles the structure content of the Sc4 conformation (Toyama et al., 2007). This structural study also opened up the possibility for differential chaperone binding playing a role in strain phenotypes. To address, this, an *in vitro* system was established to provide a framework in which to map the chaperone recognition elements on SupNM fibers. Although these works provide substantial progress into the study of prion structure, more detailed analysis will be needed to ascertain the full fiber structure. Methods such as solid-state NMR have been instrumental in achieving atomic resolution models of other amyloids. The size of SupNM would initially seem to prohibit the use of this technique, however, through new NMR techniques and labeling schemes, this barrier will hopefully be scaled in the near future.

Structural understandings in hand, we can now start to piece together the sequences of characteristics that produce the prion strain phenomenon and begin to answer Robertson's challenge. The disparity in the length of the amyloid fold between

the Sc4 and Sc37 conformations provides a structural rationale for the differences in the physical characteristics of the respective fibers. Sc37 fibers are less fragile than Sc4 fibers due to the increased number of residues that participate in the fiber fold. Thus, the smaller amyloid fold of Sc4 results in weaker, more breakable fibers, resulting in many small fibers which are more effective at recruiting and sequestering natively folded protein, which results in a minimal population of soluble and function Sup35p, causing the white color phenotype. The larger amyloid fold of Sc37 results in stronger fibers which more effectively resist shearing, resulting in fewer fibers to help recruit and sequester natively folded protein, which allows more soluble and functional Sup35p to persist, causing the pink color phenotype. More concisely, conformational heterogeneity leads to heterogeneity of physical characteristics, which leads to differing aggregation efficacies, which in the case of the yeast prion [*PSI*$^{+}$], produces distinct *in vivo* phenotypes. Indeed, there is also evidence of a strong correlation between aggregate stability and *in vivo* phenotype in the mammalian system. Here, it was demonstrated that the incubation time of the disease correlated with the stability of the aggregate, where the more easily the aggregate melted, the shorter the disease incubation time. Perhaps now, over 20 years later, endeavors into the study of prion structures have finally allowed us to demonstrate how the "structures of the prion protein…can be related to scrapie strain specificity", satisfying a lingering challenge to the protein-only prion hypothesis.

Appendix A

References

References

Alberti, S., Halfmann, R., King, O., Kapila, A., and Lindquist, S. (2009). A systematic survey identifies prions and illuminates sequence features of prionogenic proteins. Cell *137*, 146-158.

Bagriantsev, S.N., Gracheva, E.O., Richmond, J.E., and Liebman, S.W. (2008). Variant-specific [*PSI*$^{+}$] infection is transmitted by Sup35 polymers within [*PSI*$^{+}$] aggregates with heterogeneous protein composition. Mol Biol Cell *19*, 2433-2443.

Bessen, R.A., and Marsh, R.F. (1992). Identification of two biologically distinct strains of transmissible mink encephalopathy in hamsters. J Gen Virol *73 (Pt 2)*, 329-334.

Bessen, R.A., and Marsh, R.F. (1994). Distinct PrP properties suggest the molecular basis of strain variation in transmissible mink encephalopathy. J Virol *68*, 7859-7868.

Brachmann, A., Baxa, U., and Wickner, R.B. (2005). Prion generation in vitro: amyloid of Ure2p is infectious. Embo J *24*, 3082-3092.

Bradley, M.E., Edskes, H.K., Hong, J.Y., Wickner, R.B., and Liebman, S.W. (2002). Interactions among prions and prion "strains" in yeast. Proc Natl Acad Sci U S A *99 Suppl 4*, 16392-16399.

Bruce, M.E., and Dickinson, A.G. (1987). Biological evidence that scrapie agent has an independent genome. J Gen Virol *68 (Pt 1)*, 79-89.

Carulla, N., Caddy, G.L., Hall, D.R., Zurdo, J., Gairi, M., Feliz, M., Giralt, E., Robinson, C.V., and Dobson, C.M. (2005). Molecular recycling within amyloid fibrils. Nature *436*, 554-558.

Castilla, J., Saa, P., Hetz, C., and Soto, C. (2005). In vitro generation of infectious scrapie prions. Cell *121*, 195-206.

Caughey, B., and Lansbury, P.T. (2003). Protofibrils, pores, fibrils, and neurodegeneration: separating the responsible protein aggregates from the innocent bystanders. Annu Rev Neurosci *26*, 267-298.

Chernoff, Y.O., Lindquist, S.L., Ono, B., Inge-Vechtomov, S.G., and Liebman, S.W. (1995). Role of the chaperone protein Hsp104 in propagation of the yeast prion-like factor [*PSI*$^{+}$]. Science *268*, 880-884.

Chien, P., DePace, A.H., Collins, S.R., and Weissman, J.S. (2003). Generation of prion transmission barriers by mutational control of amyloid conformations. Nature *424*, 948-951.

Chien, P., Weissman, J.S., and DePace, A.H. (2004). Emerging principles of conformation-based prion inheritance. Annu Rev Biochem *73*, 617-656.

Chiti, F., and Dobson, C.M. (2006). Protein misfolding, functional amyloid, and human disease. Annu Rev Biochem *75*, 333-366.

Cohen, F.E., and Prusiner, S.B. (1998). Pathologic conformations of prion proteins. Annu Rev Biochem *67*, 793-819.

Collinge, J. (2001). Prion diseases of humans and animals: their causes and molecular basis. Annu Rev Neurosci *24*, 519-550.

Collins, S.R., Douglass, A., Vale, R.D., and Weissman, J.S. (2004). Mechanism of prion propagation: amyloid growth occurs by monomer addition. PLoS Biol *2*, e321.

Cox, B., Ness, F., and Tuite, M. (2003). Analysis of the generation and segregation of propagons: entities that propagate the [*PSI*$^+$] prion in yeast. Genetics *165*, 23-33.

Crist, C.G., Nakayashiki, T., Kurahashi, H., and Nakamura, Y. (2003). [*PHI*$^+$], a novel Sup35-prion variant propagated with non-Gln/Asn oligopeptide repeats in the absence of the chaperone protein Hsp104. Genes Cells *8*, 603-618.

Delaglio, F., Grzesiek, S., Vuister, G.W., Zhu, G., Pfeifer, J., and Bax, A. (1995). NMRPipe: a multidimensional spectral processing system based on UNIX pipes. J Biomol NMR *6*, 277-293.

DePace, A.H., Santoso, A., Hillner, P., and Weissman, J.S. (1998). A critical role for amino-terminal glutamine/asparagine repeats in the formation and propagation of a yeast prion. Cell *93*, 1241-1252.

DePace, A.H., and Weissman, J.S. (2002). Origins and kinetic consequences of diversity in Sup35 yeast prion fibers. Nat Struct Biol *9*, 389-396.

Derkatch, I.L., Chernoff, Y.O., Kushnirov, V.V., Inge-Vechtomov, S.G., and Liebman, S.W. (1996). Genesis and variability of [*PSI*] prion factors in Saccharomyces cerevisiae. Genetics *144*, 1375-1386.

Dickinson, A.G., and Meikle, V.M. (1969). A comparison of some biological characteristics of the mouse-passaged scrapie agents, 22A and ME7. Genet Res *13*, 213-225.

Dobson, C.M. (2003). Protein folding and misfolding. Nature *426*, 884-890.

Ferreira, P.C., Ness, F., Edwards, S.R., Cox, B.S., and Tuite, M.F. (2001). The elimination of the yeast [*PSI*$^+$] prion by guanidine hydrochloride is the result of Hsp104 inactivation. Mol Microbiol *40*, 1357-1369.

Fiaux, J., Bertelsen, E.B., Horwich, A.L., and Wuthrich, K. (2002). NMR analysis of a 900K GroEL GroES complex. Nature *418*, 207-211.

Glover, J.R., Kowal, A.S., Schirmer, E.C., Patino, M.M., Liu, J.J., and Lindquist, S. (1997). Self-seeded fibers formed by Sup35, the protein determinant of [*PSI*$^+$], a heritable prion-like factor of S. cerevisiae. Cell *89*, 811-819.

Goddard, T.D., and Kneller, D.G. SPARKY 3, University of California, San Francisco.

Hall, D., and Edskes, H. (2004). Silent prions lying in wait: a two-hit model of prion/amyloid formation and infection. J Mol Biol *336*, 775-786.

Hoshino, M., Katou, H., Hagihara, Y., Hasegawa, K., Naiki, H., and Goto, Y. (2002). Mapping the core of the ß$_2$-microglobulin amyloid fibril by H/D exchange. Nat Struct Biol *9*, 332-336.

Jones, E.M., and Surewicz, W.K. (2005). Fibril conformation as the basis of species- and strain-dependent seeding specificity of mammalian prion amyloids. Cell *121*, 63-72.

Jones, G.W., and Tuite, M.F. (2005). Chaperoning prions: the cellular machinery for propagating an infectious protein? Bioessays *27*, 823-832.

Jung, G., and Masison, D.C. (2001). Guanidine hydrochloride inhibits Hsp104 activity in vivo: a possible explanation for its effect in curing yeast prions. Curr Microbiol *43*, 7-10.

King, C.Y., and Diaz-Avalos, R. (2004). Protein-only transmission of three yeast prion strains. Nature *428*, 319-323.

Kochneva-Pervukhova, N.V., Chechenova, M.B., Valouev, I.A., Kushnirov, V.V., Smirnov, V.N., and Ter-Avanesyan, M.D. (2001). [*Psi*(+)] prion generation in yeast: characterization of the 'strain' difference. Yeast *18*, 489-497.

Kraulis, P.J. (1989). ANSIG: A Program for the Assignment of Protein 1H 2D NMR Spectra by Interactive Graphics. J Magn Reson *84*, 627-633.

Krishnan, R., and Lindquist, S.L. (2005). Structural insights into a yeast prion illuminate nucleation and strain diversity. Nature *435*, 765-772.

Kryndushkin, D.S., Alexandrov, I.M., Ter-Avanesyan, M.D., and Kushnirov, V.V. (2003). Yeast [*PSI*$^+$] prion aggregates are formed by small Sup35 polymers fragmented by Hsp104. J Biol Chem *278*, 49636-49643.

Kushnirov, V.V., and Ter-Avanesyan, M.D. (1998). Structure and replication of yeast prions. Cell *94*, 13-16.

Legname, G., Baskakov, I.V., Nguyen, H.O., Riesner, D., Cohen, F.E., DeArmond, S.J., and Prusiner, S.B. (2004). Synthetic mammalian prions. Science *305*, 673-676.

Liu, J.J., Sondheimer, N., and Lindquist, S.L. (2002). Changes in the middle region of Sup35 profoundly alter the nature of epigenetic inheritance for the yeast prion [*PSI*$^+$]. Proc Natl Acad Sci U S A *99 Suppl 4*, 16446-16453.

Luhrs, T., Ritter, C., Adrian, M., Riek-Loher, D., Bohrmann, B., Dobeli, H., Schubert, D., and Riek, R. (2005). 3D structure of Alzheimer's amyloid-beta(1-42) fibrils. Proc Natl Acad Sci U S A *102*, 17342-17347.

Maji, S.K., Wang, L., Greenwald, J., and Riek, R. (2009). Structure-activity relationship of amyloid fibrils. FEBS Lett *583*, 2610-2617.

Makarava, N., and Baskakov, I.V. (2008). The same primary structure of the prion protein yields two distinct self-propagating states. J Biol Chem *283*, 15988-15996.

Masel, J., Jansen, V.A., and Nowak, M.A. (1999). Quantifying the kinetic parameters of prion replication. Biophys Chem *77*, 139-152.

May, B.C., Govaerts, C., Prusiner, S.B., and Cohen, F.E. (2004). Prions: so many fibers, so little infectivity. Trends Biochem Sci *29*, 162-165.

Moriyama, H., Edskes, H.K., and Wickner, R.B. (2000). [URE3] prion propagation in Saccharomyces cerevisiae: requirement for chaperone Hsp104 and curing by overexpressed chaperone Ydj1p. Mol Cell Biol *20*, 8916-8922.

Muchmore, D.C., McIntosh, L.P., Russell, C.B., Anderson, D.E., Dahlquist, F.W., and Norman, J.O.a.T.L.J. (1989). [3] Expression and nitrogen-15 labeling of proteins for proton and nitrogen-15 nuclear magnetic resonance. In Methods in Enzymology (Academic Press), pp. 44-73.

Nelson, R., Sawaya, M.R., Balbirnie, M., Madsen, A.O., Riekel, C., Grothe, R., and Eisenberg, D. (2005). Structure of the cross-beta spine of amyloid-like fibrils. Nature *435*, 773-778.

Ness, F., Ferreira, P., Cox, B.S., and Tuite, M.F. (2002). Guanidine hydrochloride inhibits the generation of prion "seeds" but not prion protein aggregation in yeast. Mol Cell Biol *22*, 5593-5605.

Osherovich, L.Z., Cox, B.S., Tuite, M.F., and Weissman, J.S. (2004). Dissection and design of yeast prions. PLoS Biol *2*, E86.

Parham, S.N., Resende, C.G., and Tuite, M.F. (2001). Oligopeptide repeats in the yeast protein Sup35p stabilize intermolecular prion interactions. Embo J *20*, 2111-2119.

Peretz, D., Scott, M.R., Groth, D., Williamson, R.A., Burton, D.R., Cohen, F.E., and Prusiner, S.B. (2001). Strain-specified relative conformational stability of the scrapie prion protein. Protein Sci *10*, 854-863.

Pierpaoli, E.V., Gisler, S.M., and Christen, P. (1998). Sequence-specific rates of interaction of target peptides with the molecular chaperones DnaK and DnaJ. Biochemistry *37*, 16741-16748.

Prusiner, S.B. (1982). Novel proteinaceous infectious particles cause scrapie. Science *216*, 136-144.

Ritter, C., Maddelein, M.L., Siemer, A.B., Luhrs, T., Ernst, M., Meier, B.H., Saupe, S.J., and Riek, R. (2005). Correlation of structural elements and infectivity of the HET-s prion. Nature *435*, 844-848.

Robertson, H.D., Branch, A.D., and Dahlberg, J.E. (1985). Focusing on the nature of the scrapie agent. Cell *40*, 725-727.

Ross, E.D., Edskes, H.K., Terry, M.J., and Wickner, R.B. (2005). Primary sequence independence for prion formation. Proc Natl Acad Sci U S A *102*, 12825-12830.

Rudiger, S., Germeroth, L., Schneider-Mergener, J., and Bukau, B. (1997). Substrate specificity of the DnaK chaperone determined by screening cellulose-bound peptide libraries. Embo J *16*, 1501-1507.

Saborio, G.P., Permanne, B., and Soto, C. (2001). Sensitive detection of pathological prion protein by cyclic amplification of protein misfolding. Nature *411*, 810-813.

Safar, J., Wille, H., Itri, V., Groth, D., Serban, H., Torchia, M., Cohen, F.E., and Prusiner, S.B. (1998). Eight prion strains have PrP(Sc) molecules with different conformations. Nat Med *4*, 1157-1165.

Santoso, A., Chien, P., Osherovich, L.Z., and Weissman, J.S. (2000). Molecular basis of a yeast prion species barrier. Cell *100*, 277-288.

Satpute-Krishnan, P., and Serio, T.R. (2005). Prion protein remodelling confers an immediate phenotypic switch. Nature *437*, 262-265.

Sattler, M., Schleucher, J., and Griesinger, C. (1999). Heteronuclear multidimensional NMR experiments for the structure determination of proteins in solution employing pulsed field gradients. Progress in Nuclear Magnetic Resonance Spectroscopy *34*, 93-158.

Sawaya, M.R., Sambashivan, S., Nelson, R., Ivanova, M.I., Sievers, S.A., Apostol, M.I., Thompson, M.J., Balbirnie, M., Wiltzius, J.J., McFarlane, H.T.*, et al.* (2007). Atomic structures of amyloid cross-beta spines reveal varied steric zippers. Nature.

Schmid, D., Baici, A., Gehring, H., and Christen, P. (1994). Kinetics of molecular chaperone action. Science *263*, 971-973.

Shewmaker, F., Wickner, R.B., and Tycko, R. (2006). Amyloid of the prion domain of Sup35p has an in-register parallel beta-sheet structure. Proc Natl Acad Sci U S A *103*, 19754-19759.

Shkundina, I.S., Kushnirov, V.V., Tuite, M.F., and Ter-Avanesyan, M.D. (2006). The role of the N-terminal oligopeptide repeats of the yeast Sup35 prion protein in propagation and transmission of prion variants. Genetics *172*, 827-835.

Shorter, J., and Lindquist, S. (2005). Prions as adaptive conduits of memory and inheritance. Nat Rev Genet *6*, 435-450.

Silveira, J.R., Raymond, G.J., Hughson, A.G., Race, R.E., Sim, V.L., Hayes, S.F., and Caughey, B. (2005). The most infectious prion protein particles. Nature *437*, 257-261.

Smirnovas, V., Kim, J.I., Lu, X., Atarashi, R., Caughey, B., and Surewicz, W.K. (2009). Distinct structures of scrapie prion protein (PrPSc)-seeded versus spontaneous recombinant prion protein fibrils revealed by H/D exchange. J Biol Chem.

Sondheimer, N., and Lindquist, S. (2000). Rnq1: an epigenetic modifier of protein function in yeast. Mol Cell *5*, 163-172.

Sparrer, H.E., Santoso, A., Szoka, F.C., Jr., and Weissman, J.S. (2000). Evidence for the prion hypothesis: induction of the yeast [*PSI*$^{+}$] factor by in vitro- converted Sup35 protein. Science *289*, 595-599.

Sun, Z.Y., Frueh, D.P., Selenko, P., Hoch, J.C., and Wagner, G. (2005). Fast assignment of ^{15}N-HSQC peaks using high-resolution 3D HNcocaNH experiments with non-uniform sampling. J Biomol NMR *33*, 43-50.

Tanaka, M., Chien, P., Naber, N., Cooke, R., and Weissman, J.S. (2004). Conformational variations in an infectious protein determine prion strain differences. Nature *428*, 323-328.

Tanaka, M., Chien, P., Yonekura, K., and Weissman, J.S. (2005). Mechanism of cross-species prion transmission: an infectious conformation compatible with two highly divergent yeast prion proteins. Cell *121*, 49-62.

Tanaka, M., Collins, S.R., Toyama, B.H., and Weissman, J.S. (2006). The physical basis of how prion conformations determine strain phenotypes. Nature *442*, 585-589.

Telling, G.C., Parchi, P., DeArmond, S.J., Cortelli, P., Montagna, P., Gabizon, R., Mastrianni, J., Lugaresi, E., Gambetti, P., and Prusiner, S.B. (1996). Evidence for the conformation of the pathologic isoform of the prion protein enciphering and propagating prion diversity. Science *274*, 2079-2082.

Tipton, K.A., Verges, K.J., and Weissman, J.S. (2008). In vivo monitoring of the prion replication cycle reveals a critical role for Sis1 in delivering substrates to Hsp104. Mol Cell *32*, 584-591.

Toyama, B.H., Kelly, M.J., Gross, J.D., and Weissman, J.S. (2007). The structural basis of yeast prion strain variants. Nature *449*, 233-237.

Tuite, M.F., and Cox, B.S. (2006). The [*PSI*$^{+}$] prion of yeast: a problem of inheritance. Methods *39*, 9-22.

Tuite, M.F., and Koloteva-Levin, N. (2004). Propagating prions in fungi and mammals. Mol Cell *14*, 541-552.

Weissmann, C. (2004). The state of the prion. Nat Rev Microbiol *2*, 861-871.

Wickner, R.B. (1994). [*URE3*] as an altered URE2 protein: evidence for a prion analog in Saccharomyces cerevisiae. Science *264*, 566-569.

Wickner, R.B., Edskes, H.K., Shewmaker, F., and Nakayashiki, T. (2007). Prions of fungi: inherited structures and biological roles. Nat Rev Microbiol *5*, 611-618.

Wiltzius, J.J., Landau, M., Nelson, R., Sawaya, M.R., Apostol, M.I., Goldschmidt, L., Soriaga, A.B., Cascio, D., Rajashankar, K., and Eisenberg, D. (2009). Molecular mechanisms for protein-encoded inheritance. Nat Struct Mol Biol.

Yamaguchi, K., Katou, H., Hoshino, M., Hasegawa, K., Naiki, H., and Goto, Y. (2004). Core and heterogeneity of ß$_2$-microglobulin amyloid fibrils as revealed by H/D exchange. J Mol Biol *338*, 559-571.

Zhu, X., Zhao, X., Burkholder, W.F., Gragerov, A., Ogata, C.M., Gottesman, M.E., and Hendrickson, W.A. (1996). Structural analysis of substrate binding by the molecular chaperone DnaK. Science *272*, 1606-1614.

Publishing Agreement

It is the policy of the University to encourage the distribution of all theses, dissertations, and manuscripts. Copies of all UCSF theses, dissertations, and manuscripts will be routed to the library via the Graduate Division. The library will make all theses, dissertations, and manuscripts accessible to the public and will preserve these to the best of their abilities, in perpetuity.

Please sign the following statement:

I hereby grant permission to the Graduate Division of the University of California, San Francisco to release copies of my thesis, dissertation, or manuscript to the Campus Library to provide access and preservation, in whole or in part, in perpetuity.

Author Signature

August 31, 2009

Date